Tech Science Press

Fast Superfine Components and Sound Packets in Phenomena Induced by the Impact of a Drop on a Target Fluid in Quiescent Conditions

Yuli D. Chashechkin[*]

Ishlinsky Institute for Problems in Mechanics RAS, Moscow, 119526, Russia
*Corresponding Author: Yuli D. Chashechkin. Email: yulidch@gmail.com

Abstract: The structure of the flow and the acoustic signals generated by the impact of a freely falling drop of water with an underlying quiescent fluid have been investigated for droplets having diameter 0.5 cm and a contact velocity in the range $1.5 < U < 5$ m/s. The experimental study has been supported by high-resolution videos of the flow (as seen from above and from the side). The evolution of ejecta, spikes, droplets spray, cavity, splash, secondary cavity, streamer, secondary droplets and sequence of capillary waves is reported accordingly. In particular, perturbations of the smoothed free surface with transverse dimensions from 0.03 cm to 0.15 cm have been observed in the center of the cavity and at the head of a growing splash. The total duration of the fine structure's existence has been found to range from 30 to 50 ms. Related acoustic packets have been recorded by means of a measuring hydrophone and a sensitive microphone. Registered acoustic signals have revealed a high-frequency pulse associated with the primary contact and a delayed main lower-frequency packet (with a time shift ranging between 50 ms and 210 ms). The content of the acoustic signals indicates that from a large number of observed gas bubbles, only one was actually sounding. For such a case (the formation of the bubble resulting from the break of a thin air bridge), the shock generated by the fast-moving remnant of the bridge produces volumetric oscillations of the bubble. The sound stops as soon as the bubble takes a smooth elliptical or spherical shape. Several details are reported about the relationship between the generation of capillary and acoustic waves and the features of hydrodynamic flows relating to the cavity, or the formation of a splash and the flows caused by the interaction of secondary drops with the perturbed surface of the target fluid. The formation of fine flows components is associated with the release of available potential energy and the conservation of perturbations in a thin "double layer" located in proximity to the original contact surfaces.

Keywords: Liquid; drop; impact fine flow; waves; sound; energy

1 Introduction

The public interest in the physical processes caused by the impact of drops on liquid surface and forms of fluid flows, which reflected in literature, music, painting, jewelry production even in ancient times, has survived to the present day. Scientific studies of drop impact flow began relatively recently, but the scope

of work and the number of applications began to grow rapidly. The processes of the formation of cascades of vortex rings initiated by a drop of a colored liquid fell in the water, discovered in the first experiments [1], stimulated the study of other types of spatial structures of flows and the mechanisms of their evolution. Firstly, the formation of vortex rings and the subsequent cascades of vortices was visualized, and the influence of the properties of contacting liquids was studied [2]. Later, the topics of work began to expand rapidly due to the influence of a number of factors. The invention of bright spark sources of light, the improvement of the photographing technique [3], the development of optical observation methods, in particular, the creation of microscopes with a distant observation plane had a positive effect. Another valuable factor was practical importance of new physical results. During experiments on tracking the motion of microdrops in a flat capacitor, the value of the discrete electron charge was determined [4] and along the way, the well-known formula for calculating the drag on a sphere [5] was corrected.

Rayleigh's papers on the stability of liquid jets and the calculation of the frequencies of natural oscillations of drops started new way of theoretical research [6]. Slow oscillations of drops of the liquid and compound drop of immiscible liquids in gravity [7] and electrostatic fields [8] as well as high-frequency oscillations of gas bubbles emitting acoustic waves were actively studied. The sound generated by gas bubbles was firstly recorded by a microphone [9] and with the appearance of hydrophones—in a liquid bulk [10,11]. The developed early theory of gas bubbles oscillations [12] was many times confirmed in experiments. Later it was noticed, that flashes of light accompany intense forced oscillations of bubbles in an external acoustic field. The effects of sonoluminescence, both emitted by group of bubbles discovered back in the first half of the last century, and by a singular bubble, have been actively studied in recent years [13,14].

An analysis of the decay process of a charged oscillating droplet led L. Meitner and O. Frisch to the idea of constructing a "drop model of decay of the nucleus", the oscillations of which were excited by an absorbed neutron [15]. The decay of the nucleus results in the formation of large (new nucleus) and small (new neutrons) fragments that are analogues of small droplets—satellites from the remnants of the neck between separated fragments [16]. The nuclear liquid–drop model applied to radioactive decay, containing a number of empirical coefficients, successfully describes the energy and decay processes of the nuclei of a large number of elements [16] although, before the invention of high-speed video recorders [17], many of the subtle details of actual flow patterns of the breakneck remained unknown. Experiments clarifying the geometry of the processes of separation and disintegration of the drops, the dynamics of the satellites continue to be carried out rather actively and at present [18].

The list of technological applications of drip technologies has been expanding quite actively in recent years. Here, an important place is occupied by studies of the interaction of micro-drops with a solid surface in order to investigate hydrodynamic of a jet and drop contact [19] and to optimize the operation of drip printers [20]. Now the technology of drip printing is widely used in microelectronics for soldering contacts. Spray coating [21], metallurgical processes of high-intensity melting of metals and gas injection during smelting [22,23]; injection of solid particles into metal melts; gas drainage from the molten mass [24] are among fast developing technologies. Physics of a drop impact is studied to combat icing of aircraft [25].

In recent years, drip technologies applied for enhancing heat transfer and cooling processes by liquid jets and films [26] as well as by spraying the coolant at normal [27] and reduced gravity at space conditions [28]. Techniques of bubble boiling intensification was actively discussed [29,30]. Experimental results were used to develop recommendations for the prevention of fires [31,32] and improvement of volumetric explosions technologies [33]. Drip technologies are used to activate catalytic reactions by spraying the liquid phase of the reagent onto the surface of metal powders [34], for optimization of fuel injection in internal combustion engines [35].

Drops impact in the liquid is accompanied by the formation of gas bubbles [36]. The experiments clarify the spatio-temporal characteristics of the structural components of the flows, both fine (thin ejecta and lamina at the initial contact of the drop with the surface of the target liquid, sprays), and large ones that are cavities, crowns, capillary waves. In recent years, much attention has been paid to detailed analysis of the droplet matter transport in a target liquid [37]. From the review follows, that more and more attention is paid to study the fine flow structure in all phases of the process of a freely falling drop immersion and spreading in the target fluid, which is of both scientific and practical interest.

In the given paper, the data of systematical studying the fine structure evolution of the flow pattern produced by a free falling drop on the surface of a target fluid in quiescent conditions, registered by high-resolution video register and emitted acoustic packets measured by hydrophone and microphone are presented.

2 The Main Parameters of Droplet Impact Flows

Theoretical studies and parametrization of the pinch-off, motion, and immersion of a freely falling drop processes, as well as a series of subsequent rapidly changing flow patterns in a target liquid, are conventionally carried out on the basis of the fundamental equations of fluid mechanics. The basic system includes the equations of continuity, momentum and energy transfer in approximations of an ideal fluid (system of Euler equations) or taking into account the action of dissipative factors. For only viscosity effect the system of conventional Navier–Stokes equations [38,39], which are not written here for brevity, are used.

The boundary conditions on the free surface $\zeta(\mathbf{r}, t)$, which are derived from the integral formulations of the laws of conservation of the mass of the liquid and the transfer of momentum and energy, are divided into three types that are kinematic, dynamic, and energy.

The set of basic dimensional parameters of the problem includes densities of all the media involved in the processes under study (air ρ_a, drop ρ_d and the target ρ_t liquids, below noted $\rho_{a,d,t}$), kinematic $v_{a,d,t}$ and dynamic $\mu_{a,d,t}$ viscosities of media, basic σ_d^a, σ_t^a and normalized to the density of liquids $\gamma_d^a = \sigma_d^a/\rho_d$, $\gamma_t^a = \sigma_t^a/\rho_t$ cm^3/s^2 surface tension coefficients on the liquid-air contact surface, diffusion coefficient κ [38,39]. The description of experimental conditions includes the gravity acceleration g, equivalent diameter of the droplet D, height of its free fall H or drop velocity U at the time of initial contact.

The physical parameters of the environments and experimental conditions determine sets of intrinsic length and time scales, which characterize the properties of the studied problem. They are collected into several groups. In one of them, the scales depend on the physical parameters of the media, in others they depend on the size D or velocity U of the falling drop.

One group of length scales contains a capillary-gravitational parameter $\delta_g^\gamma = \sqrt{\gamma/g}$ included in the dispersion equation of short surface waves [38], and dissipative-capillary scales $\delta_\gamma^v = v^2/\gamma$, $\delta_\gamma^\kappa = \kappa^2/\gamma$. Scales widely used for parameterization, such as $\delta_g^v = \sqrt[3]{v^2/g}$, can be considered as combinations of basic scales, in particular $\delta_g^v = \sqrt[3]{\delta_\gamma^v \left(\delta_g^\gamma\right)^2}$. Another group of length scales, depending on the droplet velocity, includes Prandtl's type $\delta_U^v = v/U_d$, $\delta_U^\kappa = \kappa/U_d$ and $\delta_U^\gamma = \gamma/U_d^2$ capillary scales.

Accordingly, one group of intrinsic time scales includes only medium parameters that are $\tau_g^\gamma = \sqrt[4]{\gamma/g^3}$, $\tau_\gamma^\kappa = \kappa^3/\gamma^2$, $\tau_\gamma^v = v^3/\gamma^2$, second group contains the droplet size $\tau_\gamma^d = \sqrt{D^3/\gamma}$, $\tau_\kappa^\gamma = \kappa D/\gamma$, $\tau_v^\gamma = vD/\gamma$, the third one depends on its velocity $\tau_U^d = D/U_d$, $\tau_g^U = U_d/g$.

In low-viscosity media, the range of variability of scales is quite wide [37]. In particular, for water, the largest and smallest length scales equal $\delta_{\max} = \delta_g^\gamma = \sqrt{\gamma/g} = 0.24$ cm and $\delta_{\min} = \delta_\gamma^\nu = \nu^2/\gamma = 1.37 \cdot 10^{-6}$ cm, respectively, and the time scales are $\tau_{\max} = \tau_\gamma^d = 0.032$ s и $\tau_{\min} = \tau_\gamma^\nu = 1.9 \cdot 10^{-10}$ s.

Ratios of different spatial or temporal base scales determine a set of dimensionless combinations—numbers of Reynolds $\mathrm{Re}_d = UD/\nu_d$ characterizing the motion of a drop and $\mathrm{Re}_t = u_t L_t/\nu_t$ for flows inside the bulk of the target fluid with scales of velocity u_t and length L_t; Froude $\mathrm{Fr}_d = U^2/gD$; Weber

$$\mathrm{We}_d = U^2 D/\gamma_d; \text{ Bond } \mathrm{Bo} = D^2 \left/ \left(\delta_g^\gamma\right)^2 \right. = gD^2/\gamma_d^a \text{ and Ohnesorge } \mathrm{Oh} = \sqrt{\delta_\gamma^\nu \left/ D \right.} = \nu/\sqrt{\gamma D}.$$

The values of scales define the requirements for the experimental technique: the choice of the size of the observation field, the resolution of the optical register and the exposition time, parameters of hydrophone and microphone. The large scales flow components are easily resolved by modern experimental techniques, while small scales components of a type δ_γ^ν, whose sizes are approaching the size of a molecular cluster, cannot be resolved.

3 Technique of Experiment

The experiments performed at the Stand for the study of surface and underwater processes (ESP) as part of the USF "HPC IPMech RAS" [40]. The basis of the stand designed to study the fine structure of the surface and underwater processes by consistent optical, contact, and acoustic instruments, is a transparent Plexiglas's basin *1* with dimensions of 1.5 m × 0.4 m × 0.6 m. High-quality optical windows are inserted into side walls of the basin, which was filled with degassed tap water. A photograph of the stand is shown in Fig. 1.
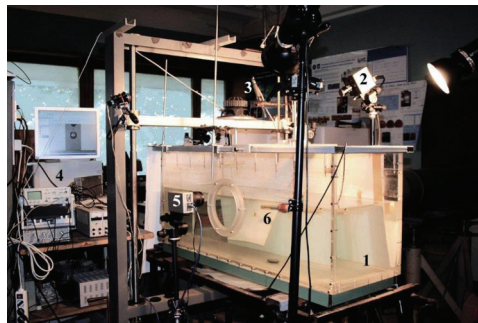

Figure 1: Experimental stand ESP

Sloping light rays of two multi-element sources of constant light MultiLED illuminated the observation area. The system of caustics in the pattern of reflected and scattered light from a multipath collimated source, forming on the free surface of a transparent liquid, visualizes capillary waves of small amplitude and steepness. The method represents the simplified realization of "the synthetic schlieren method" [41] with a multipoint source of light replacing the dot mask.

Optronis CR3000 × 2 high-speed video cameras *2*, *5* (shooting frequency is up to 20 000 frames per second, shutter speed is 1/10000 s) registered the flow pattern.

A broadband microphone *3* was placed above the basin. Measuring hydrophone *6* was installed inside the basin. Controller *4* on the quartz resonator, the signals from which were transferred to a computer, carried out the synchronization and collection of measuring systems signals, cameras, the hydrophone, and the microphone.

Above the basin at a height of 20 cm–120 cm from the surface of the target liquid, a drop dispenser was installed, which could form droplets with diameters from 0.2 cm to 0.6 cm with a prescribed frequency. Separated drops fell freely due to gravity. The drop trajectory crossed the line of sight of the optical shutter signal, which fixed its passage. The signal from the shutter fed to the input of the adjustable delay controller *4* to start the video cameras.

Digital processing of optical images and data analysis performed in a Matlab environment. The image was scaled on a grid with a step of 1.0 cm. The experimental technique and data processing were developed taking into account the requirements for recording fine details of the flow pattern (up to 12 µm) and resolution of short-lived components up to microseconds.

4 Experimental Results

4.1 Hydrodynamics of a Drop Impact

The first presented frame from the video (Fig. 2), demonstrates that drop, freely falling from the dispenser installed at a height of $H = 70$ cm, has the almost perfect shape and is slightly elongated vertically (the width and the height of the drop are $D_h^d = 0.61$ cm and $D_v^d = 0.62$ cm, respectively) right before the contact with target liquid. The dark spot in the lower right corner of the frame is the image of the hydrophone head.

In the initial phase of immersion of the droplet at $t = 0.5$ ms around the dark rim, which is the edge of the immersed drop, a thin gray translucent plane ring ("ejecta") with width $\Delta R_e = 0.76$ mm is expanded. The outer edge of fast-expanding ejecta formed by sharp narrow cusps, separated by smooth deep troughs. Thin translucent, radially oriented strokes separated by relatively wide clean spaces fly out from the tips of cusps. At this stage, the temporal resolution of the instruments does not allow to unambiguously indicate whether individual strokes are thin water jets—spikes, or a blurry image of rapidly flying droplets. Some radial spikes, which are formed by the merger of two touching sides of the cusps are clearly visible in subsequent frames.

In the next frame, when the wall of the cavity is separated from the drop edge (at $t = 1.0$ ms the width of the light ring is $\Delta R_R = 0.6$ mm), the flow velocity decreases and the identification of the structural components becomes more reliable. In the center of the image, the remnant of the impacting drop is immersing ($D_h^d = 0.60$ cm, $D_v^d = 0.58$ cm). A light ring surrounding the drop remnant is the visible part of the cavern bottom (with an outer diameter of $D_v^c = 0.8$ cm). A dark adjoining ring displays the inclined wall of the cavity and the upper edge of the growing crown. The ring contacts with an expanding translucent flat ring—lamina, with a pronounced thickening along the edge rim. On the rugged outer edge of the lamina (its width ΔR_l lies in the range from 0.78 cm to 1.51 cm) pointed cusps are expressed (there are more than 20 here, then their number decreases with time), separated by smooth deep troughs.

Thin jets flying out from the tops of cusps on the lamina edge are spikes breaking up into separate droplets. Some droplets continued spikes; some are shifted and inclined, which indicates the multiplicity of mechanisms of their generation.

Detailed examination of the enlarged image of the frame at $t = 1$ ms helps to distinguish two groups of droplets and two subsequent rings on this image. The outer lamina, where the liquid enters from the edge of the crown, is thicker and more contrasting. The primary internal ejecta, which is closer to the surface of the target fluid, is thinner and less contrast. Liquid enters into primary ejecta directly from the contact line of the falling drop and the target medium. Similar structures were visualized earlier when recording the flow induced by a drop of silicone oil or glycerol-water mixture impact in the deep layer of the same fluid [42] and reproduced numerically in [43].
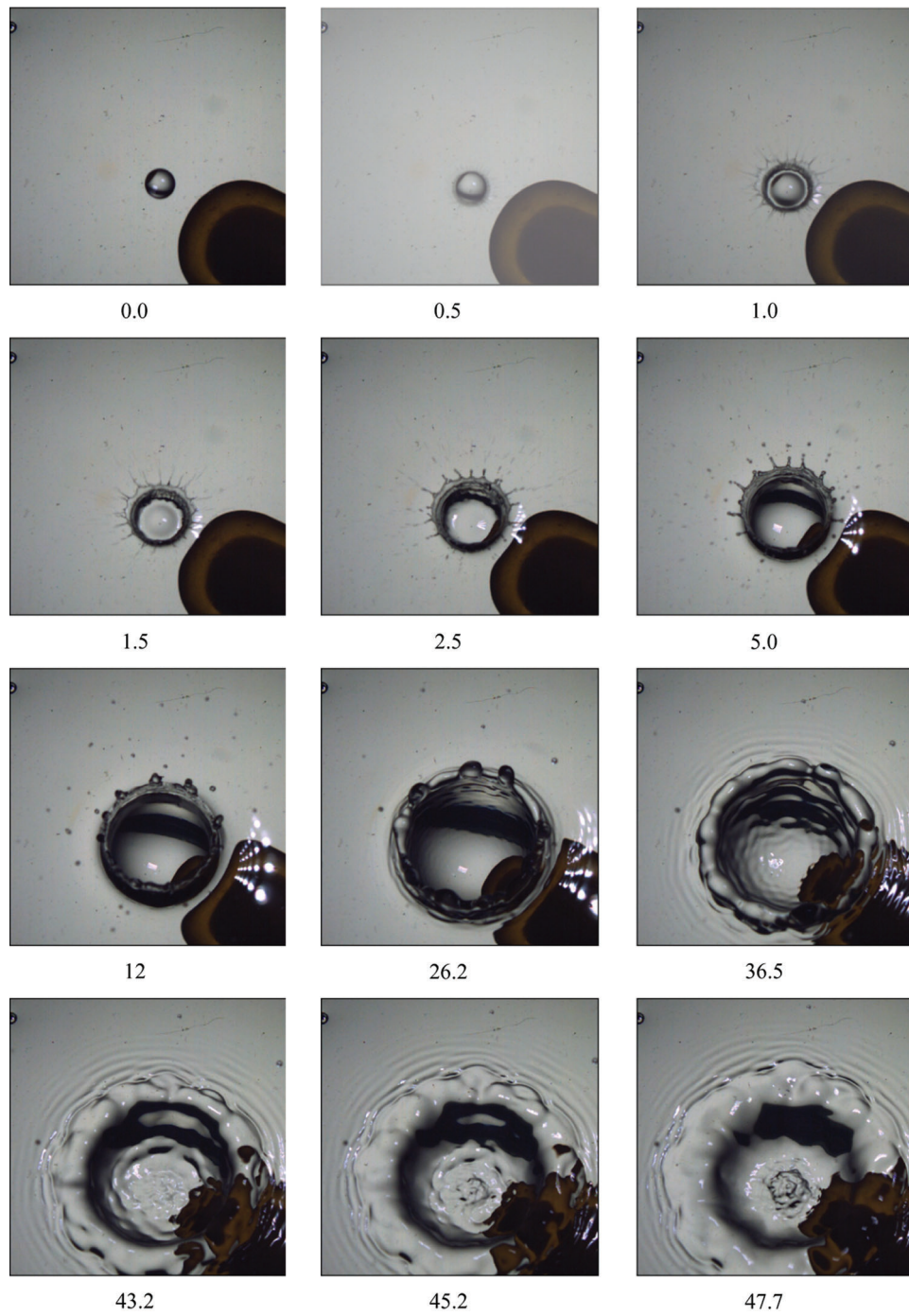
0.0

0.5

1.0

1.5

2.5

5.0

12

26.2

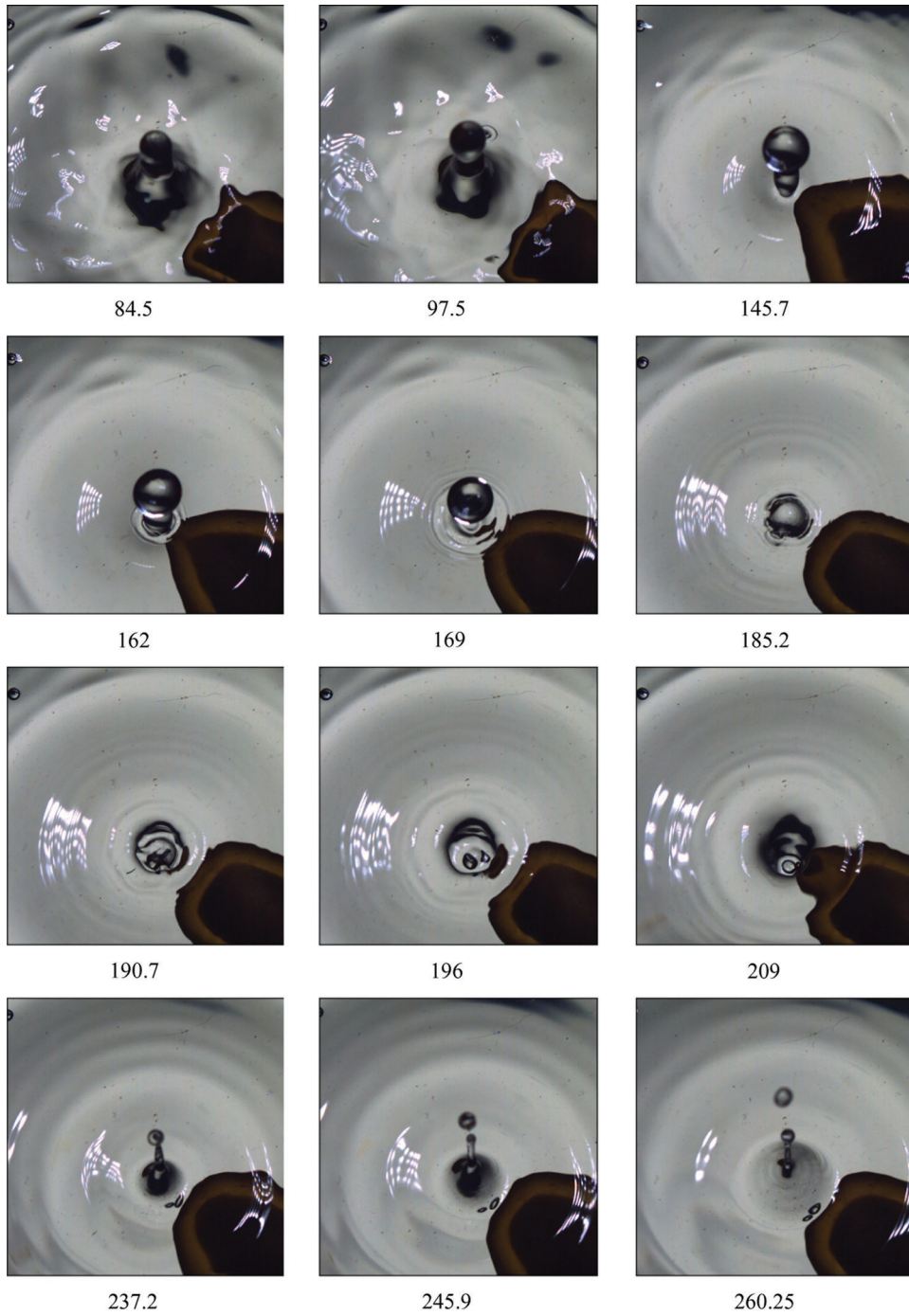36.5

43.2

45.2

47.7

Figure 2: (Continued)
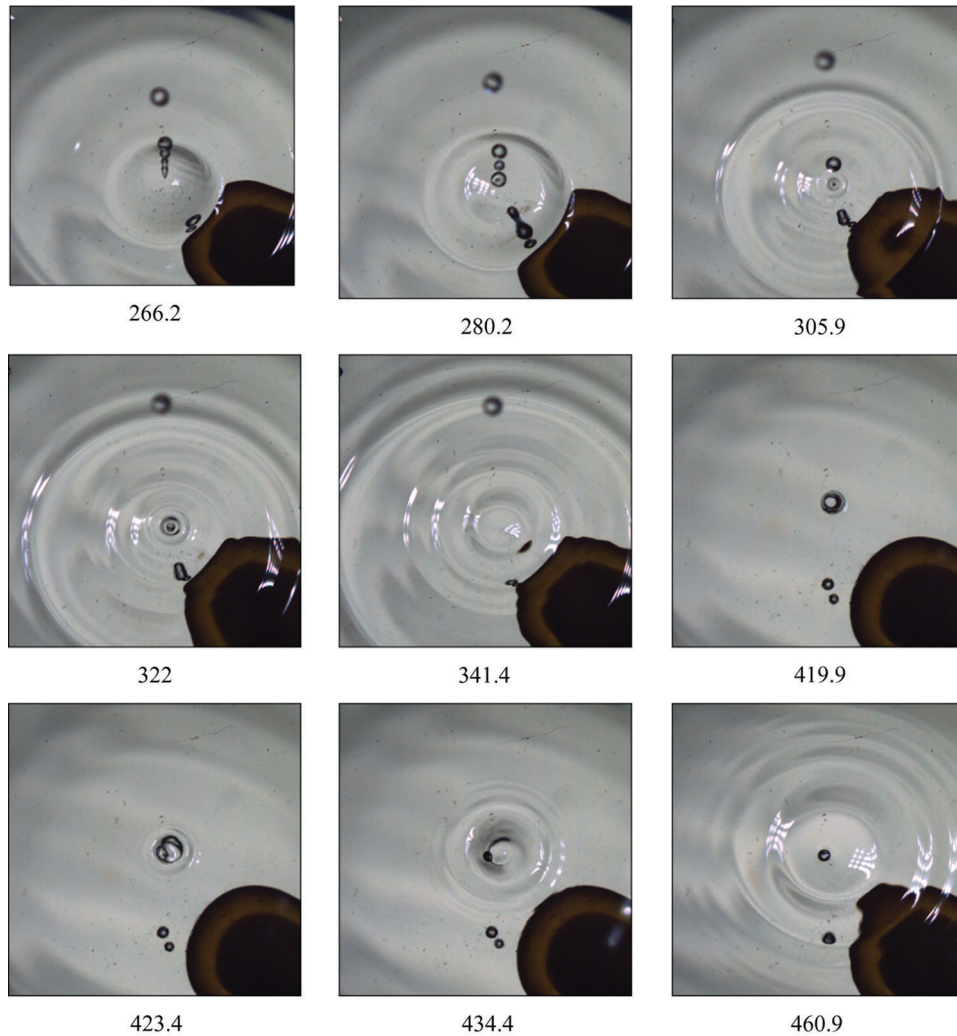
Figure 2: (Continued)

Figure 2: Video frames of flow pattern produced by a water drop impact on deep water at rest ($D = 0.6$ cm, $U = 3.7$ m/s, top view), the numbers under the photographs indicate the time in milliseconds

A complication of the flow pattern is observed in the next frame at $t = 1.5$ ms, where the width of the cavity is $D_h^c = 0.80$ cm. The thickness of the dark ring, visualizing the inclined wall of the cavity and the crest of the growing crown, is $\Delta R_w = 2$ mm. its outer edge transformed into a translucent lamina which width is $\Delta R_l = 0.78$ mm. The cusps on the outer edge of the lamina become more pronounced with time.

Thin radial jets are spikes with length from 4.1 mm to 4.8 mm, which are ejected from the tops of the cusps. Small droplets periodically fly out from the outer ends of the spikes in the radial direction. Droplets are concentrated in several thin circular zones separated by wide empty rings. The manifestation of zonal structures in the pattern of the spatial position of droplets that fly out from different separated spikes synchronously and at close velocities indicates the existence of fine trickles in the walls of the cavity and crown, and general oscillatory processes.

Over time, separate protrusions appear on the walls of the cavity with a diameter of $D^c = 0.85$ cm at $t = 2.5$ ms. They represent crests of three-dimensional capillary waves emerging from the upper edge of the by crown and going to the remnant of the primary drop with a major axis equal to $D_h^d = 0.53$ cm and a minor

axis equal to $D_v^d = 0.46$ cm on the bottom of the cavity. The distances between the peaks of the protrusions are 1 mm and 1.25 mm, their height is 0.7 mm. The wave pattern on the crown was studied in [44]. At the same time, short capillary waves of small amplitude begin to run away from the outer wall of the crown, as evidenced by the appearance of caustics (a regular set of light spots) between crown and hydrophone.

Although in the frame at $t = 2.5$ ms the remnants of a completely immersed drop are not visible, dimensions the cavity, as well as the width of the crown, are growing due to inertia. Capillary waves (similar to observed in [44]) cover the walls of the cavity, whose diameter $D^c = 0.96$ cm at $t = 2.5$ ms. Thin jets fly out from the thickened tips of the spikes with length at the range from 0.5 mm to 3 mm at the cusps of the lamina edge. With time the length of spikes decreases as separated droplets take off some matter. In the spatial distribution of the secondary droplets that have escaped from the tips of the spikes, the zonal structure is expressed. Circular slots containing droplets are separated by empty rings. With time, the strokes which lengths here are 1.52 mm, 1.53 mm, 1.61 and 1.57 mm become shorter and their diameters grow. Variations of the strokes sizes, forming the zonal structures, show that the radial velocities of the flying droplets decrease with time.

A change in the convex form of the hydrophone head image at $t = 0.5$ ms to concave at $t = 2.5$ ms and the appearance of a group of point caustics (bright light points on its image) indicates the formation of a relatively wide trough (depression) covering the domain with the crown, along the bottom of which groups of short capillary waves propagate.

The zonal structure of the pattern of droplets flying from the tops of spikes becomes more pronounced over time. At $t = 5$ ms, there are four slots where droplets are located along one of the radius vectors at distances of $R_1 = 13.36, 18.26, 22.46, 27.08$ mm, and along with the other, $R_2 = 13.10, 15.48, 19.64, 23.91, 29.63$ mm. The first groups of fast droplets have already left the field of observation. Spikes become shorter (from 0.3 to 2 mm long), some of them completely disappear, and the edge of the crown is smoothed. The synchronism of the processes of drop emitting from the tips of different spikes indicates the existence of global oscillations of the upper edge of the crown and protruding crests. The diameters of droplets here are from 0.3 mm to 0.6 mm. The bottom of the cavity, the diameter of which increases uniformly and is equal to $D^c = 1.06$ cm, remains smooth.

The systems of ring short capillary waves propagating on the surface of target liquid from the outer edge of the crown are visualized by a system of caustics that are bright light spots on a dark image of the hydrophone. Comparisons with neighbor images show that the number and size of spots, the lengths of the lightened domain, which are determined by the number, length, amplitude, and velocity of propagating waves, grow with time. The length of the shortest waves in this group is 0.5 mm, and increases to 2 mm.

The image of the hydrophone is split, the convex part of its head is located inside the image of the cavity, and the concave remainder is on the outside. The complication of the image shape is due to an increase in the amplitude of the concavity of the liquid surface outside the crown, as well as growing the lengths and amplitudes of the propagating ring capillary waves. However, their amplitudes are still so small that they do not appear in surface images and visualized by the motions of caustic points only.

At $t = 12$ ms, only twelve irregularly spaced spikes remain above the crown crest with an external diameter of $D^c = 23.9$ mm, and rather large drops fly out from the tops some of them. The successive distances between the annular rows of droplets are $R_3 = 14.84, 18.29, 22.35$ mm along one of the radius vectors, and $R_4 = 20.46, 23.60, 37.71$ mm along with the other. The number of light dots in the hydrophone image (here there are seven, in the previous frame was 5) and the size of the lightened area are progressively increasing. In the image of the free surface, ring capillary waves are not yet manifested.

With the expansion of the crown, the diameter of which reaches $D^c = 29.7$ mm at $t = 26.2$ ms, the capillary waves cover both the inner and the outer sidewalls of the crown, while the bottom of the cavity remains smooth. The upper edge of the crown is partially smoothed out, only a few protrusions with a width of 4.05 mm, 3.93 mm, 3.07 mm remain on it, the distances between their centers are 1.94 mm and 1.37 mm. The outer sidewall of the crown covered with non-uniform ridges. With an increase in their amplitudes, surface perturbations of crests of external annular capillary waves around the crown also become noticeable.

The position of the caustics in the lower right corner of the image shows that the first group of external capillary waves has reached the frame boundary. The distorted image of the leading edge of the hydrophone indicates a large steepness of the wave and the presence of amplitude modulation of the ridges with a scale of 1.2 mm. The increase in the size of the shaded area in the cavity indicates that the entire hollow around the crown continues to deepen. Only separate large droplets ejected from the tops of crown edge crests remain in the flow pattern.

With the decay of the fine components of the flows caused by the immersion of a drop, the flow pattern becomes smoother as well. The crown with an external diameter of $D^c = 32.1$ mm at $t = 36.5$ ms begins to settle down, the protrusions on its upper edge settle as well, and capillary waves become one of the main visible structure components of the flow. Now they fill all of the visible areas including the bottom and walls of the cavity, the inner and outer walls of the crown, the area around it. All wave fields, with a common ring structure, are modulated with a pitch of $\Delta l_\varphi = 0.41, 2.4, 1.91, 1.56$ mm on the outer wall of the crown, and with step from $\Delta l_\varphi = 1.15$ mm inside the cavity. A clear light line delineating the crown is evidence of the formation of a narrow trough with a pointed bottom on its outer border. With distance away from the rim of the crown, the modulation scale increases and inhomogeneities with length $\Delta l_\varphi = 10.1$ mm observed on the crest of the second external ring of capillary waves.

The complex image of the hydrophone inside the cavity is a consequence of the deep multiscale distortion of the free surface. It complements wave patterns, known from the first observations, by new details. The rugged leading edge of the hydrophone image indicates the three-dimensional nature of the near-surface flows.

Further spreading of the crown (external diameter $D^c = 35$ mm and width $\Delta R = 4.7$ mm at $t = 43.2$ ms) generating outgoing ring capillary waves as well as the collapse of the cavity are supplemented by the formation of a new structural component that is the ascending splash (Worthington's jet or cumulative jet) with its own set of small-scale surface perturbations. Simultaneously a system of fine spikes arose in the center of the upward flow. Protruding spikes (diameter of the central is $d_s = 0.65$ mm) surrounded by deep potholes, separated by ribs with sharp edges. The pattern of the flow is rapidly evolving and seems "bubbling"; subtle perturbations "emerge" from the depths and sink. The domain of their location is limited. They are placed to the central part of the flow on the head of the growing splash. Several groups of smooth capillary waves with length $\lambda_c = 1.12, 2.07, 1.85, 1.89$ mm remain between the central region and the rim of the crown with smooth ridges with width in a range from 7.0 mm to 10.1 mm.

The paradoxical appearance of new fine structural components against the background of the surface with smoothed initial perturbations indicates that for a long time there is a layer inside the liquid with intense thin flows. The layer is carried to the surface by regular gravitational-capillary inward flow supplemented outward spreading the crown.

The complexity of the picture of the hydrophone image underlines the increase in the amplitude and steepness of capillary waves. The magnitude of the modulation of the external field $\Delta l_\varphi = 7.01, 10.13$ mm reflects the heterogeneity of the shape and velocity of displacement of the outer wall of the crown.

In the next frame at $t = 45.2$ ms, when the outer diameter of the crown is $D^c = 36.92$ mm and the width is $\Delta R = 6.28$ mm, the head of the growing splash with a diameter of $D^s = 12.24$ mm is clearly defined. The

splash covered by a system of annular perturbations with pointed ridges and deep depressions, both long and short, with dimensions $\delta = 2.02, 1.95, 1.8$ mm. In the center of the angular region measuring 5.06 mm by 5.2 mm, outlined by ribbed ridges, there is a spike with diameter $\delta_s = 1.2$ mm. The original video shows that individual spikes randomly appear to grow and disappear, the depressions fill and form again, and the overall picture is constantly changing.

At $t = 47.7$ ms, when the outer diameter of the crown is $D^c = 40.47$ mm, and the width of the ridge is $\Delta R = 9.12$ mm, the fine-structure head of the growing splash with a side length of 6.75 mm is even more pronounced, while the perturbations in the surrounding trough are smoothed out. In the center of the angular region, measuring 6.75 mm and 6.5 mm, there is a spike with a diameter of $\delta_s = 0.9$ mm. The top of the growing splash is covered by a system of annular perturbations with pointed ridges and deep depressions with length $\delta = 2.02$ mm, 1.95 mm, 1.8 mm and separated from the crown by an annular depression with smooth surface perturbations.

On the edge of the crown, there are only pointed depressions. Small-scale perturbations are preserved here only at the leading edge of the hydrophone image, which falls on the boundary of the growing splash.

Then, the monotonous evolution of the formed structural components continues, and at $t = 51.5$ ms the outer diameter of the crown is $D^c = 5.23$ cm and its width is $\Delta R = 9.91$ mm. Continuing to grow in the center of the trough, the splash takes a cylindrical shape with a diameter of $D^s = 9.44$ mm. The scales of pronounced perturbations on its surface are $\delta = 0.63, 0.66, 1.04$ mm. The diameter of the central spike is $\delta_s = 0.6$ mm is smaller than in the previous frame, despite the smoothing effect of viscosity. The sharpening of structure can be explained by the emergence on the surface of a layer with an even finer structure of flows from the depth of the liquid. The size of the annular cavity outlining the base of the splash is $d_s = 0.94$ cm, the diameter of the region of the maximum depth of the trough between the splash and the remnant of the crown is $d_d = 2.04$ cm.

At 52.7 ms, the diameter of the crown, the outer edge of which went beyond the frame, is 51.31 mm, the diameter of the inner edge is 19.09 mm, and the brightly lit annular depression is 11.13 mm. The head of the splash has grown and slightly thinned; its diameter is now equal to 0.9 cm. The structure of perturbations on the splash surface has changed. Now they have the form of steps with a size of 0.67, 0.94, 1.34, 1.62 mm. A conical pedestal formed between the structured head and the bottom of the central trough. The diameter of its base that is a brightly lit annular depression is 1.9 cm. The bottom of the trough is smooth, on the surface of the remainder of the crown, there are gentle protrusions (length in azimuthal direction is 10.4 and 10.8 cm) and narrow depressions.

In the interval 0.78 ms between the previous and analyzed frames (60.5 ms), small-scale perturbations disappeared in the flow pattern. The surface and the peak of the splash become smooth, the dark base of which has a diameter of 12.5 mm, and a spreading crown with an outer diameter of 6.01 cm and an inner diameter of 4.79 cm. The bottom of the trough covered with wide protrusions of arbitrary shape and narrow depressions, some of which are oriented in radial directions, some troughs are located at an angle to the local radius vector.

At $t = 84.5$ ms, when the inner diameter of the crown is $D^c = 6.1$ cm, the splash becomes the main structural element of the flow. The jet consists of a smooth spherical head with a diameter of $D_s^d = 0.62$ mm, turning into a cylindrical section, which rests on a conical pedestal with a base diameter of $d_d = 1.4$ cm. A system of troughs of a spiral shape with a characteristic scale of $l_t = 4.68$ mm is suitable for the base. The shape of the hydrophone shadow indicates an increase in large-scale deformations of the liquid surface and the appearance of intermediate troughs.

Over time, the height of the conical base, cylindrical section, and the diameter of the spherical tip of the splash increase uniformly ($t = 97.5$ s) and fine structure features decay in all components of the flows. Past the splash, there is a small circular hole—the annular trail left by the fallen droplet, which was previously

ejected by one of the streamers on the outline of the crown. At the last stage of crown development, the orientation of the streamers, which ejected droplets, was close to vertical.

By the moment $t = 145.7$, a significant part of the splash had flowed into the central drop, the diameter of which is now equal to $D_s^d = 9.74$ mm. As the fluid inflow velocity decreases, the conical base begins to thin (here its diameter in the area of contact with the target fluid is only 2.28 mm). Next, the remnant of the splash begins to sink, not having the energy to completely separated away from the target fluid. A change in the direction of motion of the splash is accompanied by the generation of a new group of short capillary waves of small amplitude. They are not visualized in surface displacements directly but are manifested in the structures of ring caustics on the right and left, as well as in the change in the entire light field around the splash.

When a splash is immersed, ring short capillary waves form both in the surrounding trough and directly on its lateral surface ($t = 162$ ms). A droplet with a diameter of $D_s^d = 0.97$ cm falls more slowly than a splash. The thickness of their contact area and the radius of curvature of the liquid surface in the zone begins to decrease rapidly, which leads to the appearance of a bright caustic under the droplet.

Within 7 ms (at $t = 169$ ms) the central part of the splash manages to break away from a slowly sinking drop with a diameter $D_s^d = 0.92$ cm, and completely sink, forming a conical cavity. When the surface of the target liquid is closed after immersion of the peak of the splash, a group of ring capillary waves is formed, the length of which decreases with distance from the source and is $\lambda_r = 2.21, 1.99, 0.79, 0.75$ mm. The crests of the waves, like other phase surfaces, are rather deeply modulated.

In the next frame at $t = 185.2$ s, the enlarged image clearly shows that as a drop with a diameter of $D_s^d = 0.82$ cm is in contact with only separate points on the perturbed surface of the target liquid, several air cavities appear. Two round cavities placed on the left and bottom, as well as two elongated, locate on the bottom right and top left. In this case, new ring capillary waves with a length of $\lambda_r = 0.99$ and 0.91 mm appear. The waves of the group represented in the previous frame run away at distances of $R = 15.0$ mm. 17.9 mm, 19.9 mm, 21.6 mm, 22.8 mm.

Upon further immersion of the droplet at $t = 190.7$ s, in the cavity with $D_s^c = 8.6$ mm in diameter, several gas bubbles become trapped. The largest bubble, which placed in the center of the flow, has a diameter 6.0 mm, smaller bubbles are in the bottom and on the top right. The bubbles change their shape and actively move under the influence of buoyancy forces, the attraction of the free surface and the action of fast internal flows.

At the same time, new groups of capillary waves of greater length and amplitude are formed, as can be seen from the shape of the surface itself and the distorted image of the hydrophone. The waves of the packet that arose during the immersion of the droplet moved away to a distance of $R = 8.57$ and 9.9 mm, and when the liquid surface was closed after immersion of the remnant of the splash, to a distance of $R = 17.05, 20.3, 22.81, 24.73$ mm.

Some dark spots in these images are parts of the hydrophone image caused by the deflection of light rays due to large three-dimensional variations of the surface slopes and height. These perturbations are not visible with applied visualization technique in given and several subsequent frames ($t = 196$ s and $t = 209$ s), when the conical cavity closes and the groups of capillary waves propagate. Gas bubbles of conical shapes with sizes 3.65 mm $\times$ 2.66 mm and 2.63 mm $\times$ 1.87 mm at $t = 196$ ms are located in the center of a cavity with a diameter of $D^c = 8.53$ mm. The cavity actively collapses, and at $t = 209$ ms its diameter is 4.46 mm. In the center of the cavity, there is a spherical bubble with a diameter of 2.28 mm, to which a smaller bubble adjoins to the right.

By the time $t = 237.2$, when the cavity is completely collapsed, a fast, thin, vertically oriented jet that is a streamer is ejected. A droplet with a diameter $d_{st} = 3.2$ mm is ready to fly out into the air from the streamer

top. The streamer rests on a conical pedestal with a base diameter of 7.6 mm. From the whole set of gas bubbles, only two close-together bubbles of dimensions 2.1 mm × 0.9 mm and 2.9 mm × 1.35 mm right to the bottom at a distance of $R = 6.3$ mm from the streamer center are preserved in the field of view.

By the time of $t = 245.9$ ms, the upper droplet with a diameter of $d_{st} = 3.64$ mm breaks off the top of the streamer and a new one begins to form in its place. Gas bubbles are separated by a distance of $\Delta L_g = 0.5$ mm and are somewhat removed from the center of the flow (the distance between the centers of flow and bubbles is $R_b = 7.5$ mm and 7.7 mm).

Gradually, the base of the pedestal begins to expand and cover by short capillary waves. The drop-off droplet actively oscillates, which is manifested in the variability of its diameter equal to $d_{st} = 3.73$ mm at 260.2 ms, the droplet diameter at the top of the streamer is $d_{st}^2 = 2.94$ mm. Bubbles move rather randomly, get closer and diverge.

An upward moving streamer at $t = 266.2$ ms separates from the oscillating surface of the liquid, in which the sinking pedestal forms a new cavity, and begins to decay into four connected droplets of various shapes and diameters (successively close to spherical diameters of $d_g = 2.87$ mm, 2.09 mm and elongated pear-shaped dimensions 1.45 mm × 1.77 mm and 1.28 mm × 2.12 mm). The upper drop assumes a nearly spherical shape with a diameter of $d_g^2 = 3.8$ mm. Bubbles diverge and are $\Delta R_g = 10.2$ mm from the center for small and $\Delta R_g = 11.75$ mm for large.

The lower droplets falling under the action of gravity into the liquid form new small caverns surrounded by groups of diverging ring waves, and new gas bubbles. The diameters of droplets in the assembly are $d_{st} = 3.0$ mm and 2.03 mm at $t = 280.2$ ms. The submerging lower droplet forms a cavity with a diameter of 2.8 mm. The shape of the oscillating upper drop noticeably differs from the spherical one. The contacting bubbles form a pear-shaped assembly oriented in the radial direction with a total length of 8.9 mm. Now only two droplets are observed in the flow pattern (the lower with a diameter of $D_s^c = 2.9$ mm) and the cavity with a diameter of $D_s^c = 2.1$ mm, surrounded by a new group of capillary waves.

At $t = 305.9$ several remote groups of diverging waves arising from the contact of an immersed droplet with a liquid and the collapse of another conical cavity are observed. Formed fine trickles in the flow actively change the position and shape of gas bubbles. Here there are two sticking bubbles together and one disconnected.

The next submerging droplet with a diameter of $d_{st} = 2.9$ mm at $t = 322.9$ ms falls exactly in the center of the cavity remaining from the previous droplet, which explains the axial symmetry of the observed capillary wave pattern. The flows create a new configuration of a group of merged gas bubbles with dimensions of 3.21 mm × 2.17 mm and 1.64 mm × 0.69 mm an apparent decrease in size of which is due to stretching in the vertical direction.

At $t = 341.4$ ms, the next falling drop with a diameter of $d_{st} = 4.34$ mm is visible. All surface of the target fluid is coved by groups of short capillary waves. The pattern of light caustics visualizes their internal structure formed by waves lengths $0.5 < \lambda_c < 2.5$ mm. Separated gas bubbles of size 3.21 mm × 2.17 mm and 1.64 mm × 0.69 mm have an axially elongated shape.

On a smoothed observable surface completely freed from capillary waves at $t = 419.9$ ms, a cavity with a diameter of $D^c = 4.34$ mm and two gas bubbles of a spherical shape with a diameter of $d_b = 2.33$ mm and 1.93 mm are observed.

As the droplet sinks, a new complex structure formed by deformed gas bubbles is observed in the cavity with a diameter of $D^c = 4.76$ mm inside of the rim with diameter $D^r = 6.7$ mm in the center of flow at $t = 434.4$ ms. The large gas fragment of complex form is placed in the central part of the cavity. An elongated gas hollow with dimensions of 2.34 mm × 1.57 mm adjoins the lift side of the cavity. The diameters of spherical gas bubbles near the hydrophone are $d_b = 2.14$ mm and 1.92 mm. With time, bubbles on the periphery of the

flow begin to converge. During the cavity collapse, the new groups of annular capillary waves are actively generated.

At the last stage of the active evolution of the flow, one of the gas bubbles, transporting by remnants of flows remains in the center of the flow. Bubbles on the periphery also merged into one with a diameter of $d_b = 2.35$ mm.

An analysis of the images shows the active role of the fine components of the flows at the initial stage of the evolution of the flows, accompanied by the rapid spreading of the immersing primary drop in the stationary target fluid at $t < 5$ ms, then at the beginning of the splash formation at 43.2 ms $< t < 60.5$ ms and at the final stage of the flow evolution at $t > 260.2$ ms, when they manifest itself in the formation of groups of short capillary waves, as well as severe deformation and intense transport of gas bubbles. The processes of contact, fusion, and pinch-off of gas cavities are accompanied by the emission of sound wave packets.

For a more complete description of the geometry of the three-dimensional flow, Fig. 3 shows the results of lateral video recording of a three-dimensional cavity formed by a drop contacting with a target fluid. The resolution here is lower than in case of the free surface observation from above, due to losses during the propagation of light through the contact surfaces of the tank optical windows and on the optical path in water, the refraction in the regions of the capillary raising of the water surface near the tank wall. These images do not contain fine details like videograms, given in Fig. 2, nevertheless the obtained data allow clarifying important features of the subsurface flows.

Due to the shadowing of the image caused by capillary uplift, the first stages of the drop immersion in target fluid are invisible in this experiment. In the first image in Fig. 3 at 4 ms, a growing cavity with a flat bottom with depth $h_c = 3.7$ mm and diameter $D^c = 9.8$ mm is shown. As follows from data of similar experiments performed in other projections the drop by this moment has already immersed. The flat bottom of the cavity does not reproduce the initial distribution of the pressure created by the spherical drop submerging, which might be caused by the unperturbed transfer of the drop momentum at the target liquid. The flat shape of the bottom indicates the need to search for a mechanism for the accelerated distribution of drop substance and the momentum associated with the matter along the bottom of the cavity.

The bottom of the cavity with and a diameter of $D^c = 16.4$ mm and the depth of $h^c = 10.4$ mm at $t = 18.5$ ms accepts already a spherical shape but its form is not smooth. At the bottom of the cavity, there are appearing individual protrusions up to $\Delta h_p = 0.53$ mm high. They were previously identified as the crests of the high capillary waves [44]. Above the cavity, there is a crown with a height of $h^{cr} = 3.1$ mm in this projection.

By inertia, after immersion of a drop, the cavity continues to increase in size and at $t = 24.5$ ms its diameter is $D^c = 17.6$ mm and depth is $h^c = 11.7$ mm. Dark and light bands on the contour of the cavity corresponding to the crests and troughs of the waves, cover the entire surface of the cavity. The external contour of the cavity is perturbed as well.

In course of time, under the action of buoyancy forces and surface tension, the cavity begins to collapse and at $t = 31.5$ ms the diameter and depth of the conical cavity are $D^c = 17.8$ mm and $h^c = 8.9$ mm. Roughness in the bottom reflects the large steepness of the capillary waves in the cavity. At the same time, the height of the settling crown decreases.

The process of reducing the depth of the cavity proceeds simultaneously with an increase in the diameter of the crown, which at $t = 35.3$ ms is $D^c = 17.8$ mm and $h^c = 8.94$ mm. The collapse of the cavity is accompanied by the formation of thin converging flows, which further increases the perturbations of the cavity bottom. Subsequently, at $t = 39.0$ s, the bottom of the cavity with a diameter of $D^c = 18.95$ mm and a depth of $h^c = 7.0$ mm is smoothed out and takes on a convex shape again. Converging flows carry
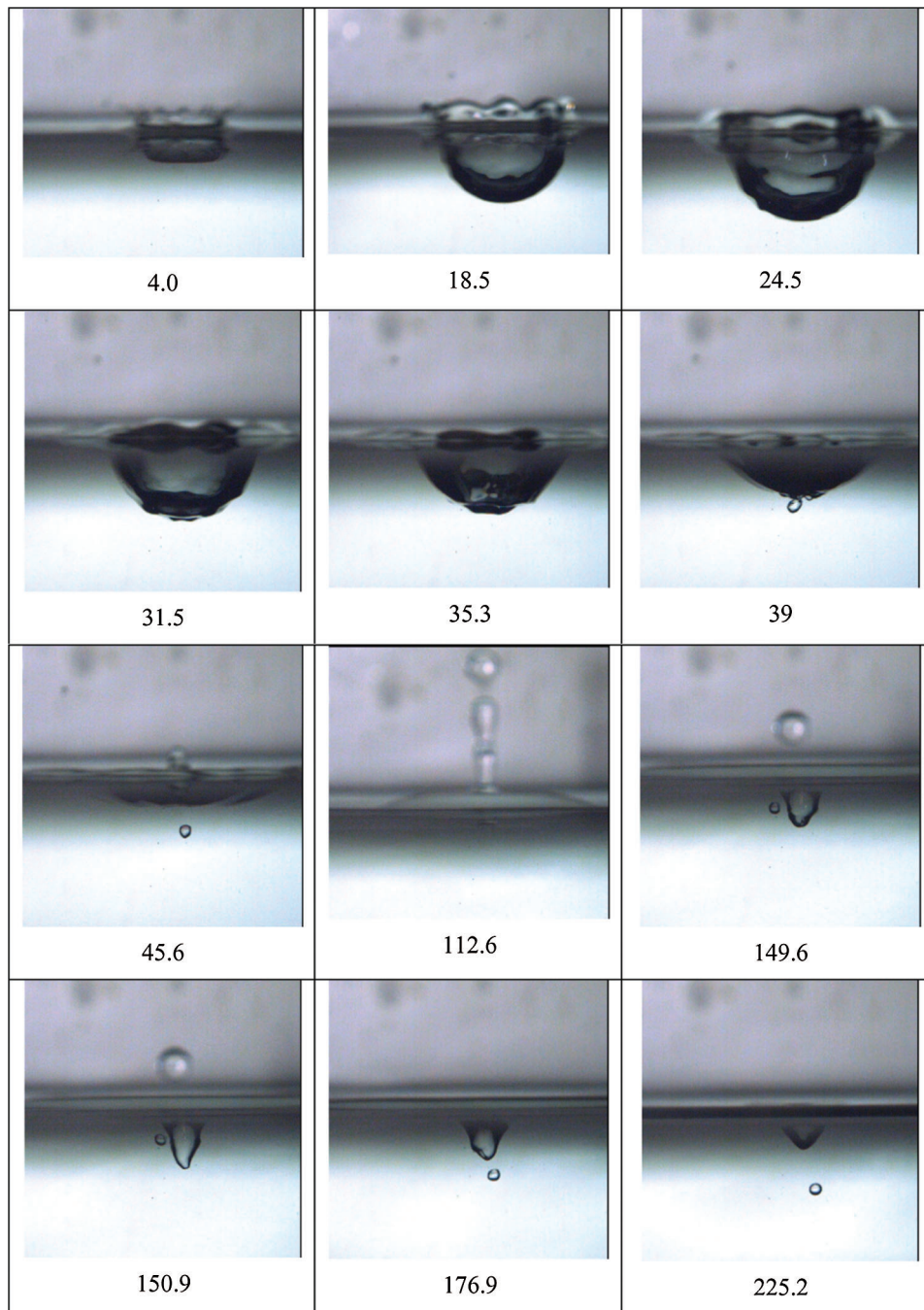
Figure 3: Video frames of a cavity created by a fallen drop of water ($D = 0.5$ cm, $U = 1.9$ m/s), the numbers under the photographs indicate the time in milliseconds

to the center of the cavity a group of deformed gas bubbles (dimensions of the largest of them are 1.7×1.3 mm), which were probably earlier in the subsurface layer and were not visible due to refraction of the light rays in the layer of capillary liquid raising.

Active subsurface flows again deform the bottom of the cavity, which at $t = 45.6$ ms becomes flat and has a diameter $D^c = 20.2$ mm and the depth $h^c = 3.85$ mm. A splash with height $h^s = 3.2$ mm and diameter

$d^s = 2.5$ mm is formed in the center of the flow. Only one vertically elongated gas bubble with dimensions of 1.42 mm $\times$ 1.26 mm remained in the center of the view field.

With enlarging the image, sharp depressions and smooth ridges at the bottom of the trough inside the remnants of the crown are visualized. Most of the gas bubbles went to the subsurface layer and only one deformed with size 1.42 mm $\times$ 1.26 mm was detached from the cavity wall and remained in the field of view.

By the time $t = 112.6$ ms, the grown splash had broken up into three fragments: the upper one is the almost regular spherical shape with a diameter of $d^s = 4.25$ mm and two elongated fragments with a height of $h^s = 5.23$ mm and a diameter of $d^s = 3.5$ mm, as well as $h^s = 4.1$ mm and $d^s = 2.29$ mm. The configuration is rested on a ring pedestal with a height of $h^p = 1.93$ mm and a diameter $d^p = 26.6$ mm. The gas bubble leaves the field of view.

The sinking fragments of the splash form in the center at $t = 149.6$ s instead of a spreading pedestal a conical cavity of not quite regular shape with a depth of $h^c = 6.5$ mm and a base of $d^c = 4.8$ mm. To the left of the cavity is a gas fragment with dimensions of 1.37 mm $\times$ 1.4 mm, close to those observed at $t = 45.6$ ms. To the right of the cavity is a small bubble with $d^b = 0.16$ mm.

On the next three frames, at $t = 150.9$ ms, 176.9 ms and 225.2 ms, the depth of the cavity with dimensions of $d^c \times h^c = 5.25$ mm $\times$ 7.73 mm, 5.8 mm $\times$ 6.8 mm, gradually decreases and deformed shape gradually accept the conical form. Intense small-scale flows deform the walls of the cavity: at $t = 150.9$ ms a flattened area is observed on its right wall, and at $t = 176.9$ ms is on the lower part of the left wall. The gas cavity of irregular form with dimensions of 1.35 mm $\times$ 1.47 mm transforms into a bubble with a diameter $d^b = 1.4$ mm, retaining its location in the center of the flow. The set of small bubbles leaves the field of view.

From the analysis of the geometric features of the given sample of frames presented in Fig. 3, it follows that the "correct" shape of the primary cavity with a spherical bottom exists for a short time in the microsecond interval. At the very beginning of the drop submerging, the bottom of the cavity is flat. At large times, its shape is distorted by general flow, capillary waves escaping from the crown and by small-scale intense trickles, expressed even at the end of the phase of active flow evolution, when a secondary cavity close to conical shape collapses with the formation of a streamer a thin fast jet flying out in the air.

The main features of the flow structure preserved when a drop of water free falls into deep water from a height of $H = 1.2$ m are given in Fig. 4. Under the conditions of the experiment, the available potential surface energy $E_s = \sigma S_d = 56.5$ erg remains unchanged, but the kinetic energy of the approaching drop $E_D = 1.54 \cdot 10^4$ erg increases noticeably ($E_s/E_D = 0.36\%$).

As in the previous case, the bottom of the cavity in the phase of immersion of the drop is flat. The shape of the cavity at the initial stages of the spreading process of the droplet is maintained until it is completely immersed. In this case, the dimensions of the cavity, the radius of the local rounding of the transition of the bottom into cylindrical walls, and the height of the crown increase monotonously. At and $t = 3.0$ ms, the depth of the cavity is $h_{ca} = 4.5$ mm, its diameter is $D^c = 11.5$ mm, and the height of the crown is $h_{cr} = 4$ mm (Fig. 4).

The inner diameters of the crown with a height of $h_{cr} = 11.1$ mm and the cavity coincide, the thickening of the crown is provided by viscous entrainment of the target fluid. Under the action of capillary forces, the crown contracts, the diameter of its serrated edge becomes smaller than the size of the cavity. Further, the cavity width continues to increase by inertia (at $t = 39.6$ ms, $D^c = 28.5$ mm, depth is $h_{ca} = 11.6$ mm) and the crown height is only $h_{cr} = 4.6$ mm. It should be noted, that for all frames of this videogram, perturbations of the walls of the cavity remain shadowed and do not appear on the presented images.
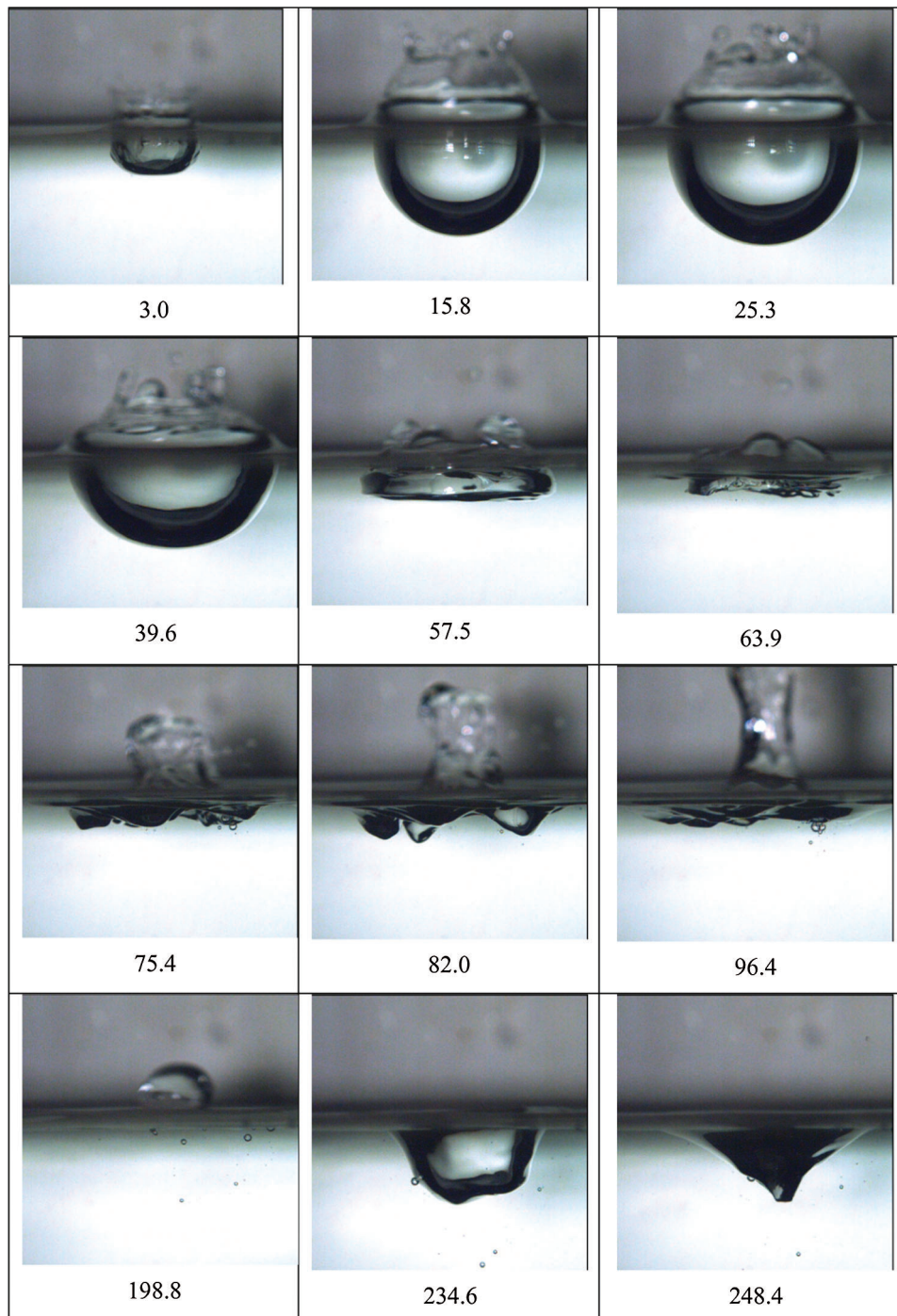
Figure 4: Video frames of a cavity created by a fallen drop of water ($D = 0.5$ cm, $U = 4.85$ m/s), the numbers under the photographs indicate the time in milliseconds

As the cavity collapses, its shape changes again, in particular, the bottom becomes flattened (the visible width is $D^c = 25.11$ mm and the depth is only $h_{ca} = 5.0$ mm at $t = 57.5$ ms). Subtle perturbations, which appeared in the flow pattern and on the inner surface of the cavity, clearly visible at high magnification of the image. The crown here is collapsed almost completely, with the exception of individual troughs. On the free

surface, there are deep "potholes" and "knolls" up to 3 mm high. There are few small gas bubbles in the view field.

Further, the shape of the cavity is transformed from a cylindrical with a flat bottom to a spherical one and at $t = 15.8$ ms its diameter is $D^c = 22.5$ mm and its depth is $h_{ca} = 13.3$ mm. Fine perturbations at $t = 63.9$ ms, in the phase preceding the start of splash growth, cover almost the entire surface of the cavity with a diameter of $D^c = 20.35$ mm and a depth of only $h_{ca} = 2.7$ mm. With a large magnification of the image, one can distinguish both elongated (linear) and "point" (spike-like) perturbations. Individual gas bubbles of various sizes appeared near the bottom of the cavity.

Over time, the severity of the cavity shape perturbations increases in which, at $t = 75.4$ ms, deep smooth depressions up to $\Delta h = 5$ mm deep appear and short ribs, protrusions, and irregular potholes remain (central is $\Delta h = 4.4$ mm deep, right is $\Delta l = 7.75$ m long and $\Delta h = 3.9$ mm deep, trench depth left side of the image is $\Delta h = 4.7$ mm). Under the center of the cavity near the depressions in the right part, groups of gas bubbles with a diameter of $d_b = 0.93$ mm, 0.45 mm, 0.19 mm and smaller are observed. Above the liquid surface, a splash with height $h_s = 10.8$ mm and diameter $d_s = 11.7$ mm was formed, the uneven surface of which was covered with tubercles and depressions.

As the splash grows (at $t = 82$ ms, its height is $h_s = 14.9$ mm and its diameter is $d_s = 8.7$ mm), the uneven nature of the surface is preserved only in its upper part, the conical lower one is smoother. The cavern bottom became smooth; it has four trenches (on the left, 5.6 mm deep and 8.7 mm wide, then 6.4 mm and 4.5 mm wide, the central one, 4.1 mm deep and 13.8 mm wide, and 5.4 mm and 10.5 mm wide on the right). The activity of subsurface flows is also evidenced by the variability of the positions and sizes of gas bubbles, the diameter of the largest of them being $d_b = 0.45$ mm.

With an increase in the height of the splash, at $t = 96.4$ ms the diameter of its central cylindrical part is $d_s = 6.8$ mm and the depth of the underwater part of the perturbations, which include seven pointed trenches with a depth starting from the left $h_t = 3.8$, 4.2, 3.57, 2.78, 4.03, 3.6 mm with relatively smooth sides, decreases. A new group of gas bubbles appears under the right trench, as attached to the surface of the liquid as drifting inside its bulk.

During the interval between consecutive frames, by the time $t = 198.8$ ms, the splash managed get completely immersed, and a droplet with a diameter of $d_d = 10.2$ mm and a height of $h_d = 6.4$ mm approached the surface of the liquid, in the bulk of which only individual gas bubbles are presented. An immersed drop pushes through the surface of the target liquid and, by the time of $t = 234.6$ ms, a cavity accepts a form of a truncated cone of an irregular shape with a base diameter of $d_c = 21$ mm and a depth of $h_c = 10.7$ mm. Small-scale disturbances cover surface of the cavity. A gas bubble is observed on the left sidewall of the cavity at a depth of $h_b = 7.1$ mm.

Under the influence of fast flows, capillary tension, and buoyancy forces, the cavity contracts into a cone with flat piecewise smooth walls and at $t = 248.4$ ms its diameter is $D_2^c = 28.2$ mm and its depth is $h_c = 9.5$ mm. The bubble also approached the free surface; its center is located at a depth of 6.7 mm. At the final collapse of a cavity of this shape, a thin energetic jet—streamer ejected into the air. The streamer shown in Fig. 2 existed at the time interval $237.2 < t < 266.2$ ms.

Conducted experiments with a high spatial and temporal resolution confirmed the known basic forms of the structural components of the flows caused by the drop impact on the motionless liquid and reliably showed the existence of fine components at all stages of flow evolution. Small radial flying droplets were observed in the phase of the primary contact of the drop with the target liquid surrounds the thin disc ejecta with cusps on the outer edge. At the drop immersion stage, the bottom of the deepening cavity contoured by a protruding crown is flat at the given regime. On the upper edge of the crown, crests were formed, ending in thin jets—streamers. New droplets fly out from the tops of streamers, the diameter of which grows with time and the flight velocity decreases. The walls of the cavity and the crown covered

by a family of three-dimensional capillary waves running down from the upper edge of the crown to the center of the cavity bottom. In the phase of the formation of a cumulative splash in the center of the trough, the surface of the liquid was covered with thin spikes and depressions. In the splash immersion phase, the bottom of the cavity takes a complex shape, including large depressions, protrusions, and small perturbations. The secondary cavity also has a complex shape.

At all stages of evolution, there existed small-scale components of the flows—short capillary waves on the surface and fast thin trickles that change the shape of the secondary cavity, the position and shape of gas bubbles in the bulk of the target fluid are observed.

The variety and complexity of the processes reflected in the graphs of changes in the diameter (curve I) and depth (curve II) of the cavity formed by free fallen drop impact on a motionless fluid from time, which are shown in Fig. 5.
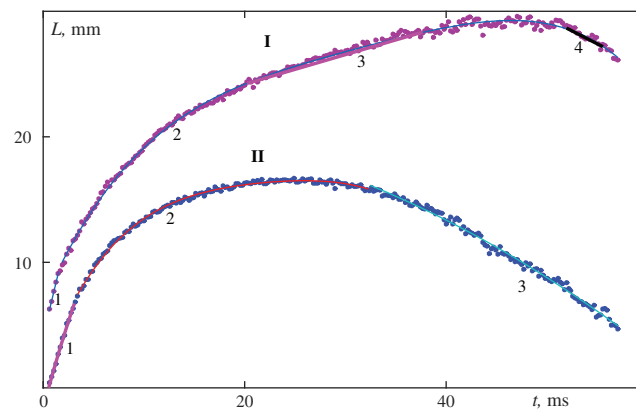

Figure 5: Evolution of the cavity sizes (curve **I**–width, curve **II**–depth) produced by water drop impact ($D = 0.5$ cm, $U = 4.85$ m/s)

At the initial stage of the drop immersion, the horizontal and vertical dimensions of the cavity $[L] =$ mm grow linearly with time $L_{xz}^1 = A_{xz}^1 + B_{xz}^1 t$, where the coefficients $A_x^1 = 4.11$; $B_x^1 = 3.35$ at 0.61 ms $< t <$ 1.75 ms and $A_z^1 = -1.32$; $B_z^1 = 2.63$ at 0.61 ms $< t <$ 3.2 ms. After immersion of a half drop, the form of the curves changes and, over a long transition interval, the experimental points are approximated by fourth-order curves $L_{x,z}^{(2)} = A_{xz}^{(2)} + B_{xz}^{(2)} t + C_{xz}^{(2)} t^2 + D_{xz}^{(2)} t^3 + E_{xz}^{(2)} t^4$, where $A_x^{(2)} = 6.847$, $B_x^{(2)} = 1.814$, $C_x^{(2)} = -0.07237$, $D_x^{(2)} = 0.001489$, $E_x^{(2)} = -1.179 \cdot 10^{-5}$ for horizontal size of the cavity over the interval 1.8 ms $< t <$ 20.2 ms and $A_z^{(2)} = 1.493$, $B_z^{(2)} = 2.119$, $C_z^{(2)} = -0.1225$, $D_z^{(2)} = 0.00344$, $E_z^{(2)} = -3.877 \cdot 10^{-5}$ for cavity depth in the interval 3.4 ms $< t <$ 32.4 ms.

Then, over the interval 37.8 ms $< t <$ 51.9 ms the horizontal size of the cavity increases linearly with time $L_x^{(3)} = A_x^{(3)} + B_x^{(3)} t$, where $A_x^{(3)} = 0.234$; $B_x^{(3)} = 19.51$. The cavity depth decreases progressively $L_z^{(3)} = A_z^{(3)} + B_z^{(3)} t + C_z^{(3)} t^2$, where $A_z^{(3)} = 21.39$, $B_z^{(3)} = 0.004976$, $C_z^{(3)} = -0.005141$ over the interval 32.5 ms $< t <$ 60.0 ms.

At the last stage of the cavity evolution at 52.0 $< t <$ 55.6 ms the horizontal size decreases linearly $L_x^{(4)} = A_x^{(4)} + B_x^{(4)} t$, where $A_x^{(4)} = 49.99$; $B_x^{(4)} = -0.4106$. The non-uniform character of curves I, II indicates action of different physical factors governing the sizes variations and a change in the dominant one at phases of their growing and decreasing. The diameter of the cavity at all stages of flow evolution exceeds its depth, although the momentum of the drop moving in the air has only vertical component.

Neglecting the presence of linear sections, both sets of experimental data are well described by fourth-order curves (with a 95% confidence interval) $L_{xz}^{(5)} = A_{xz}^{(5)} + B_{xz}^{(5)}t + C_{xz}^{(5)}t^2 + D_{xz}^{(5)}t^3 + E_{xz}^{(5)}t^4$ where the approximation coefficients of the horizontal size are $L_x^{(5)} = A_x^{(5)} + B_x^{(5)}t + C_x^{(5)}t^2 + D_x^{(5)}t^3 + E_x^{(5)}t^4$, где $A_x^{(5)} = 6.847$, $B_x^{(5)} = 1.814$, $C_x^{(5)} = -0.07237$, $D_x^{(5)} = 0.001489$, $E_x^{(5)} = -1.179 \cdot 10^{-5}$, and for the vertical are $A_z^{(5)} = 1.4936.847$, $B_z^{(5)} = 2.119$, $C_z^{(5)} = -0.1225$, $D_z^{(5)} = 0.00344$, $E_z^{(5)} = -3.877 \cdot 10^{-5}$, in the entire time interval.

The oscillatory nature of the variability of the cavity sizes is illustrated by graphs of the differences between the true values of the dimensions and interpolation curves $L_{xz}^{(5)}$ in the interval $34\,\text{ms} < t < 54\,\text{ms}$ for the horizontal and vertical sizes are presented in Fig. 6.
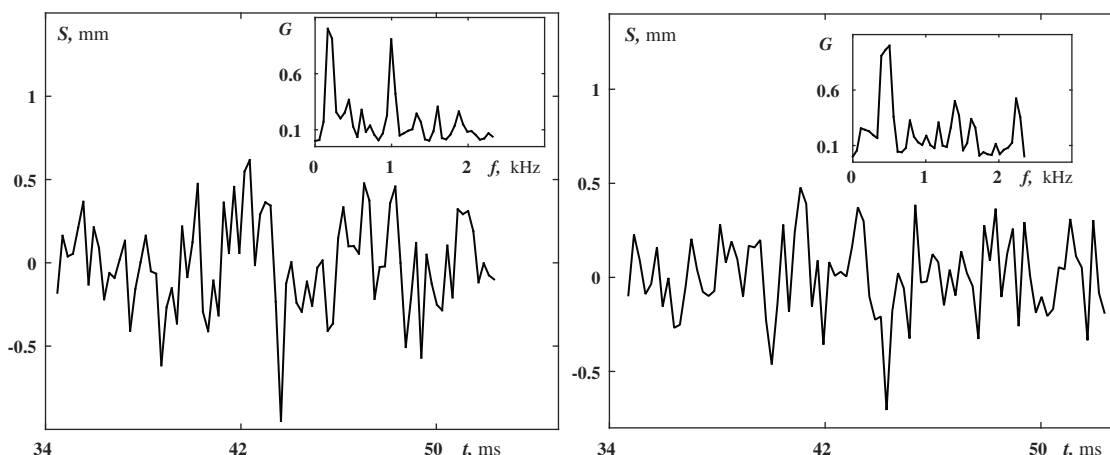

Figure 6: Temporal variability of the difference between the measured and interpolated values of the horizontal and vertical sizes of the cavity in the phase of growth and collapse of the cavity and their energetic spectra

The insets in the figures show the energy spectrum of deviations of real values from interpolation $G(f)$, calculated by the formula $G(f) = \dfrac{\Delta t}{N}\left|\sum_{n=0}^{N-1} s_n e^{-i2\pi fn}\right|^2$, where f is the frequency; $\Delta t = 1$ μs is time step here; n, N are current number and total number of samples, s_n is current deviation value.

Peaks at a frequency of 168, 995, 1600, and 1880 Hz are highlighted in the spectrum of horizontal-size variations, and for the vertical size at frequencies of 503, 1400, 2240 Hz, illustrate the propagation of capillary waves, presented in flow patterns shown in Figs. 2–4 and general oscillations of the cavity.

Important features of the applied experimental technique that are bright "multipoint" light sources, fast video recording, careful tuning of lenses helped to visualize and register fine short-lived but stably reproduced structural components of flow, which were not previously studied. Spikes in the phase of the onset of grows of the splash after smoothing of the liquid surface, thin fast trickles near cavities, which pinch-off, deform, and actively transport gas bubbles in the bulk of the liquid and short capillary waves are among them. Besides the ring capillary waves around the crown, there are several systems of short capillary waves formed in the center of the flow when the splash, streamer, and previously ejected secondary drops immersed. Moreover, the measurements show that besides the capillary waves packets of high frequency acoustic waves were generated as well.

4.2 Acoustic Wave Packets Accompanying Drop Impact

Synchronized outputs of hydrophone (Section **A**) and microphone (Section **B**) are shown in Fig. 7. At the time of the falling drop contacts with the undisturbed water surface, simultaneously with the ejection of thin circular ejecta with spikes and secondary droplets, the acoustical pulse I with a sharp positive leading edge is emitted. The amplitude of acoustic pressure is $P_a = 9.3$ Pa, the front duration (at the level of 0.7) is 7 µs, and the rising rate is $dP_a/dt = 1.15$ Pa/µs. An expanded image of the leading edge is shown in the Inset a.
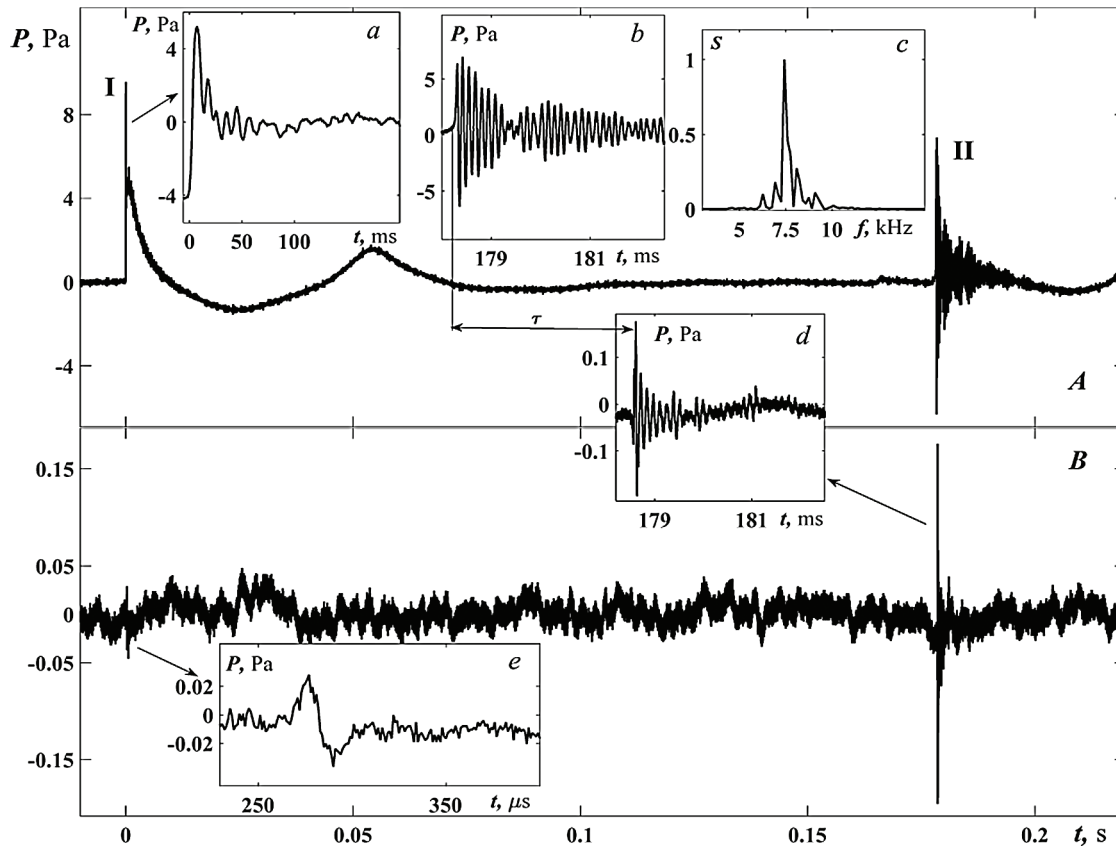

Figure 7: Hydrophone (upper section **A**) and microphone signals (lower section **B**) produced by singular drop impact ($D = 0.5$ cm, $U = 4$ m/s) with insets containing separate stretched sections of the signals and spectra of the indicated parts

The initial jump is followed by a twofold decrease in the pressure amplitude, which then oscillates with a high frequency. In the given hydrophone signal, along with the short high-frequency component of $f = 84$ kHz (it is represented by the first two oscillations), there is a longer component of $f = 45$ kHz lying on the boundary of the microphone working band. The ratio of the spectral peaks of these components is 0.25. According to signal processing data, the law of decay of the observed oscillations frequency is close to an exponential with a time constant of $\tau_d = 550$ ms. The oscillation frequencies of the primary hydrophone signal vary from experiment to experiment: oscillations with frequencies in the range $90 < f < 140$ kHz adjoin the front, and then oscillations in the range $40 < f < 80$ kHz follow.

The primary signal at the microphone, the stretched image of which is shown in Inset e, appears with the delay of 250 µs after the initial front of the hydrophone signal. The delay equals exactly to the difference in the propagation times of the sound from the contact point of the drop to the microphone and hydrophone respectively, taking into account the velocity of sound propagation in water and air. Due to the limited

microphone bandwidth, the signal does not have a pronounced leading edge, but harmonic oscillations with a frequency of $f = 45$ kHz, which are also present in the hydrophone signal, are expressed. The envelope of the oscillations is represented by an exponential with a time constant of $\tau_d = 100$ μs.

After the intense initial pulse, acoustic signals from the sensors do not arrive; all observed transient signals are caused by variations of the free surface level.

The main packet **II,** which is appeared with a delay of $\tau = 0.179$ s is present in signals from both the hydrophone and the microphone. Stretched fragments of the main signal from the hydrophone and microphone are shown in insets b and d in Fig. 6. Here the sound pressure rises rapidly (during two oscillations) and then fades. The unevenness of the acoustic pressure is more pronounced. The spectrum of the signal from the hydrophone (inset c in Fig. 7) shows oscillations with a frequency of $f = 7.6$ kHz, the signal duration to complete attenuation is $\Delta t = 30$ ms, and the exponential decay time constant is $\tau_d = 900$ μs. The signal consists of a group of packets, which can also be interpreted as modulation, the average frequency of which, estimated from the side frequencies in the signal spectrum, is 600 Hz. From experiment to experiment, the frequency of the main signal varied in the range of $4 < f < 30$ kHz. With an increase in the frequency of the observed oscillations, the duration of the full signal is significantly reduced, and modulation sharply decreases.

The initial section of the main microphone **II** signal also contains the main packet of oscillations with a frequency of $f = 7.6$ kHz, which decays exponentially with a time constant of $\tau_d = 720$ μs for $\Delta t = 1.5$ ms. Further, new increases and decreases in amplitude were observed, which can be characterized as modulation with an average frequency of $f_m = 600$ Hz.

A small number of packets in the acoustic signal presented in Fig. 7 indicates that most of the observed gas bubbles in Figs. 2–4 are "silent bubbles", which do not emit acoustic waves. The observation is confirmed by a set of phonograms obtained in repeating the experiment under constant conditions, shown in Fig. 8.
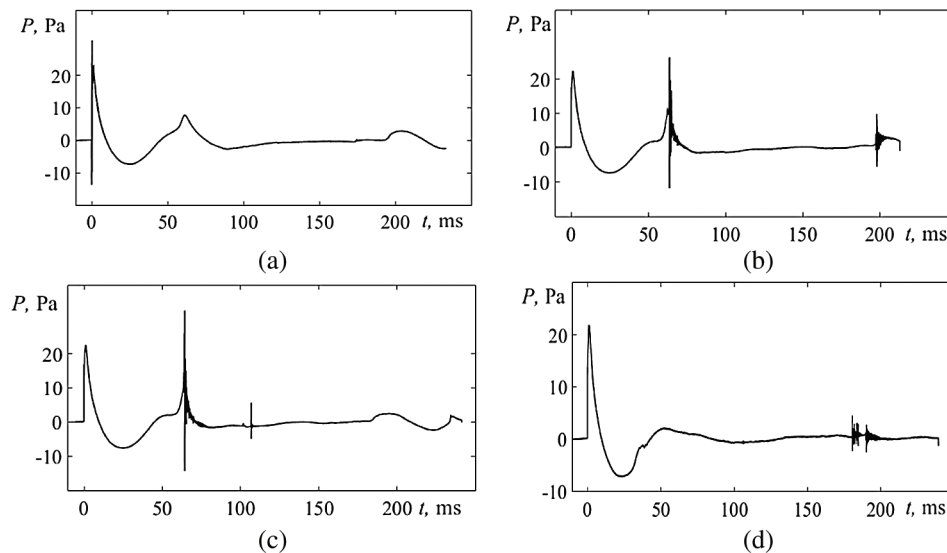

Figure 8: A sequence of phonograms accompanying the drop impact into deep water ($D = 0.5$ cm, $U = 4$ m/s)

All signals, except for the first (Fig. 8a), contain a short shock pulse arising at the moment of contact of the immersing drop with the surface of the target water, and main acoustic packets. After a steep front pulse follows a depression reflecting the formation of a cavity, which is replaced by a rise in level due to the

formation of a splash, followed by irregular low-frequency pressure oscillations of hydrodynamic nature. Against their background, short high-frequency packets are observed in the phase of the splash formation (Figs. 8b and 8c), or in the immersion of the first secondary drop and the formation of a thin streamer (Figs. 8b and 8d) or in the phase of immersion of the splash head (Fig. 8c).

Detailed observations made earlier [45,46] showed that acoustic oscillations occur when the gas cavity is separated with the formation of a thin neck, which breaks with the producing of pointed conical residues. The conical remnants of the neck quickly drawn into the new gas cavities. The shock produced by collapse of pointed conical residue of the torn neck excites the volumetric oscillations of the formed closed gas fragment. The main frequency of the sound is well described by the known formula for equivalent spherical volume oscillations [12]. An analysis of these experiments and a large number of phonograms of the process showed that bubble detachments with the formation of a long and thin neck can occur at any phase of the evolution of the flow, but most often with a delay from 0.17 s to 0.22 s. The time corresponds the interval when the prime droplet, which was previously ejected from the tip of the splash, came back and contacted the perturbed surface of the target fluid.

In a number of experiments, additional delayed acoustic packets were observed at time intervals corresponding to the fall of smaller droplets ejected from the top of the central streamer onto the surface of the target liquid. Separations of gas fragments from the deformed cavity, as well as ruptures of gas bubbles in the bulk of a liquid, are caused by the action of fast fine trickles in subsurface flows on running capillary waves.

The impact of trickles that are presented by thin and fast filaments in flow images is clearly illustrated by the fibers patterns of the coloured drop substance distribution in the target fluid. A substance of a uniformly colored drop (in the given experiment a dilute solution of alizarin ink) is concentrated in fine fibers (Fig. 9).

In the compose photograph on the left side of Fig. 9a, in the lower part of which an inverted image of the lower side of the free surface is shown, the dye is concentrated in thin fiber loops. The dyed loops form a complex pattern, which is deformed by a large component of the flows, and is rapidly changed. In a side view in the same phase of the flow in Fig. 9b around the base of the pedestal, which hides the loops visible in Fig. 9a, there are two groups of paired filaments radially directed that are short and long length. At the tops of long filaments, there are small vortex rings.
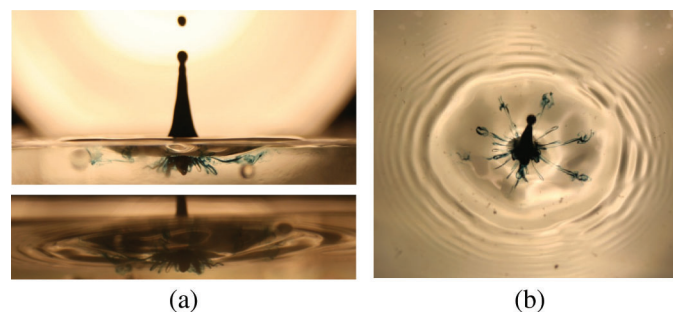

(a)   (b)

Figure 9: Pattern of flow filaments from the of the drop substance (well-mixed diluted ink solution in water) inside the target fluid in the phase of the growing splash: (*a*) side view and bottom view of the deformed free surface, (*b*) top view

The simultaneous existence of fibers of different length confirms the existence of slower and faster thin components of the flows in the bulk of the liquid, analogues of spikes in the air at the initial stage of immersion of a drop. In more detail, the pattern of the flow and transport of a colored substance of the primary drop was analyzed in [47].

5 Mechanism of Fine Flow Structure Formation

The theoretical basis of fluid mechanics is a system of fundamental equations for the transfer of matter, momentum, and energy [38,39]. In general, all components of the energy are taken into account that are potential energy, the kinetic energy of the flow and the internal energy, which is described by scalar potentials. The set of potentials includes the internal energy, enthalpy (thermal function), Helmholtz free energy and Gibbs potential (free enthalpy). Differentials of potentials determine the traditional thermodynamic parameters of the medium, in particular, the differential of the Gibbs potential determines entropy and density, energy—temperature and pressure, Helmholtz potential–entropy and pressure. The modern definitions of conventional physical quantities that are density, pressure, temperature, and others based on potentials. Functional relationships between thermodynamic quantities forming a set of state equations, are given in a series of works International Association for the Properties of Water and Steam (IAPWS) [48].

The differential of the Gibbs potential $dG_s = -sdT + VdP$, which depends on variations of temperature T and pressure P, defines entropy $s = -\left(\dfrac{\partial G_s}{\partial T}\right)_P$ and $\rho = \dfrac{1}{V} = \left(\dfrac{\partial G_s}{\partial P}\right)_T^{-1}$ explicitly and implicitly—other thermodynamic parameters.

Traditionally, the additional surface pressure proposed by P.-S. Laplace characterizes the surface tension of the interface between contacting media. Later Gibbs [49] described the boundary between media as a new surface phase and inset additional term into internal energy, in a supplement to the potential of the bulk phase. This term is now explained as a manifestation of anisotropy of atomic-molecular interactions on the contact border, which are differed from isotropic interactions in the bulk of the liquid. Upon deformation of the boundary with a change in the area of the contact surface dS_b, additional work is produced $dA = \sigma dS_b$, where σ is the surface tension coefficient.

In modern physicochemical hydrodynamics by the methods of optical and X-ray reflectivity and refractometry, spectroscopy and atomic force microscopy [50] was established that the density, dielectric constant, dipole moment are differed in the bulk of the liquid and in the structurally separated layer with a thickness of the order of 250 nm. The thickness of the liquid boundary with gas or solid, that is the order of the molecular cluster size [51].

In this layer, the Gibbs potential has a form $dG_s = -sdT + VdP - S_b d\sigma$, where the last term describes available surface potential energy, which can be transformed in other forms. Elimination of the free surface of immersing drop occurs very fast ($\Delta t_r = \delta_c/U \sim 10^{-8}$ s for conditions of given experiments) due to the small thickness of the subsurface layer $\delta_c \sim 10^{-6}$ cm. The transfer of the falling drop kinetic energy takes more time as the duration of complete immersion of the drop is longer than 1 ms.

The released surface energy, which is "frozen" in a thin "double layer" near the disappeared contact surfaces, creates large perturbations of temperature and pressure, accelerating local flows. Over time, the layer thickness increases due to the viscous diffusion of the momentum and the involvement of a thicker layer of the adhering fluid into the motion. The released energy transported away by produced flows as well as emitted capillary and sound waves. With time, the energy of fluid motions is disappeared due to the viscous dissipation.

The initial release of surface energy occurs at the contact patch of the surfaces of the drop and the target fluid. The actual size of the contacting surfaces area determines the amount of released energy. The action of the mechanism of available potential surface energy release continuing during the fusion of contact surfaces. The duration of phase of fusion, which is determined by the time of the whole drop immersion, that is, by the drop size and contact velocity $\Delta t_i = D/U \sim 10^{-3}$ s, provides long-term maintaining the large spreading velocity of the fluid in the double layer and fast growing of the cavity diameter in this observations.

Processes in a thin layer with a thickness δ_c determine the geometry of the pattern of the distribution of the droplet substance in the target liquid and on the inner surface of the "double-layer" of the growing crown as well. Formed individual "fast fibers" support process of cusps formation and elongation of spikes on the edge of the growing crown, as well as the ejection of small droplets from their tips. The dissipative increase of the thickness of the energy-saturated double layer explains the decrease in speed and the increase in the diameter of the spray formed by small droplets flying from the tips of the spikes with time. The zonal distribution structure of droplets indicates the existence of radial periodic motions that are uniform in the horizontal plane.

High-energy "double-layers", which are formed upon the immersion of each new droplet, including that ejected from the top of the splash or streamer, support fine fast flows in the target liquid. Small trickles transport bubbles from the near-surface layer into the bulk of the fluid, deforms the cavity, as well as pinch-off gas cavities from its walls, deforming gas fragments and dividing gas bubbles, accompanied by radiation of sound pulses.

It should also be underlined that thin jets (ligaments or trickles) are an important part not only drop impact flows but all fluid flows and described by singular perturbed solutions of the system of fundamental equations both in linear and non-linear approximations [52].

6 Conclusion

Consistent investigations of hydrodynamic and acoustic processes induced by impact of the free-falling drop on a deep fluid at rest were performed in the laboratory basin. A high-resolution top and side video registration of flow patterns revealed fine trickles formed during the drop immersion. Evolution of ejecta, cavity, crown with cusps on its the upper edge with attached spikes as well as a set of spikes at the stage of the splash formation and degradation was traced. New fine jets are formed during the impact of secondary drops. Formation of secondary cavities and a streamer is supplemented by generation of short capillary waves and intensive subsurface flows.

Localized regions of small-scale fluctuations, distorting the shape of the free surface at the phase of splash formation, reflect the complex pattern of energetic fine flows under the target fluid surface.

In the experiments performed, a complex structure of acoustic signals was traced by a hydrophone in water and microphone in air. Initial a shock sound packet was generated at the contact of a drop with target liquid. Resonating gas cavities emitted the main sound packets. The spectral composition of acoustic signals includes both high-frequency (about 100 kHz) and low-frequency (about 1 kHz) components. In the studied range of experimental conditions, the shock pulse repeated stably. The reproducibility and amplitude of resonant sound packets non-monotonously depend on the drop height.

The fact of the existence of fine flows in different phases of the drop immersion, spreading, the formation of cavity, splash and secondary cavities with streamer reflects the multiscale exchange processes between different components of the total energy that are the kinetic energy of the flows, potential and internal energy, including available surface potential energy.

The formation of fine flow components is associated with the fast release of available potential energy in the process of contacting fluids fusion due to the elimination of the free surface and the conservation of perturbations in a thin "double-layer".

Conflicts of Interest: The author declares that he has no conflicts of interest to report regarding the present study.

References

1. Rogers, W. (1858). On the formation of rotating rings by air and liquids under certain conditions of discharge. *American Journal of Science and Arts, Second Series, 26,* 246–258.

2. Thomson, J., Newall, H. (1885). On the formation of vortex rings by drops falling into liquids, and some allied phenomena. *Proceedings of the Royal Society of London, 39,* 417–436.

3. Worthington, A. (1895). *The splash of the drop.* series "The romance of science". New York, USA: E. & J. B. Young & Co.

4. Millikan, R. (1910). A new modification of the cloud method of determining the elementary electrical charge and the most probable value of that charge. *Philosophical Magazine, 19,* 209–228.

5. Stokes, G. (1851). On the effect of the internal friction of fluids on the motion of pendulums. *Transactions of the Cambridge Philosophical Society, 9,* 8–106.

6. Rayleigh, B., Strutt, J. W. (1877, 1878). *The theory of sound.* vol. I, II. London, England: Macmillan and Co.

7. Chekifi, T., Dennai, B., Khelfaoui, R. (2017). Computational investigation of droplets behaviour inside passive microfluidic oscillator. *Fluid Dynamics & Materials Processing, 13(3),* 173–187.

8. Esmaeeli, A., Behjatian, A. (2017). A note on the transient electrohydrodynamics of a liquid drop. *Fluid Dynamics & Materials Processing, 13(3),* 143–153.

9. Jones, A. (1920). The sound of splashes. *Science, 52(1343),* 295–296. DOI 10.1126/science.52.1343.295.

10. Pumphrey, H., Crum, L., Bjorno, L. (1989). Underwater sound produced by individual drop impacts and rainfall. *Journal of the Acoustical Society of America, 85(4),* 1518–1526. DOI 10.1121/1.397353.

11. Prosperetti, A., Oguz, H. (1993). The impact of drops on liquid surfaces and the underwater noise of rain. *Annual Review of Fluid Mechanics, 25(1),* 577–602. DOI 10.1146/annurev.fl.25.010193.003045.

12. Minnaert, M. (1933). On musical air-bubbles and the sound of running water. *Philosophical Magazine, 16(104),* 235–248.

13. Gaitan, D. F., Crum, L., Church, C., Roy, R. (1992). Sonoluminescence and bubble dynamics for a single, stable, cavitation bubble. *Journal of the Acoustical Society of America, 91(6),* 3166–3183. DOI 10.1121/1.402855.

14. Brenner, M., Hilgenfeldt, S., Lohse, D. (2002). Single-bubble sonoluminescence. *Reviews of Modern Physics, 74 (2),* 425–484. DOI 10.1103/RevModPhys.74.425.

15. Meitner, L., Frisch, O. (1939). Products of the fission of the uranium nucleus. *Nature, 143(3620),* 471–472. DOI 10.1038/143471a0.

16. Bohr, N. (1936). Zakhvat neytrona I stroyeniye yadra. *Physics-Uspekhi (Advances in Physical Sciences), 16,* 425–435 (in Russian) = Bohr N. Neutron capture and nucleus structure.

17. Thoroddsen, S., Etoh, T., Takehara, K. (2008). High-speed imaging of drops and bubbles. *Annual Review of Fluid Mechanics, 40(1),* 257–285. DOI 10.1146/annurev.fluid.40.111406.102215.

18. Chashechkin, Y. D., Prokhorov, V. (2016). Transformation of the bridge during separation of a droplet. *Journal of Applied Mechanics and Technical Physics, 57(3),* 402–415. DOI 10.1134/S0021894416030032.

19. Zhang, C., Wu, M. (2019). An analysis of the stretching mechanism of a liquid bridge in typical problems of dip-pen nanolithography by using computational fluid dynamics. *Fluid Dynamics & Materials Processing, 15(4),* 459–469. DOI 10.32604/fdmp.2019.08477.

20. Zable, J. (1977). Splatter during ink jet printing. *IBM Journal of Research and Development, 21(4),* 315–320. DOI 10.1147/rd.214.0315.

21. Mehdi-Nejad, V., Mostaghimi, J., Chandra, S. (2003). Air bubble entrapment under an impacting droplet. *Physics of Fluids, 15(1),* 173–183. DOI 10.1063/1.1527044.

22. Liow, J., Dickinson, W., Allen, M., Gray, N. (1995). Study of slopping and splashing in a cylindrical bath with top submerged injection. *Metallurgical and Materials Transactions B, 26(4),* 887–889. DOI 10.1007/BF02651734.

23. Liow, J., Gray, N. (1996). Experimental study of splash generation in a flash furnace. *Metallurgical and Materials Transactions B, 27,* 633–646.

24. Liow, J. (2001). Splash formation by spherical drops. *Journal of Fluid Mechanics, 427,* 73–105. DOI 10.1017/S0022112000002500.

25. Jin, J., Virk, M. (2018). Study of ice accretion along symmetric and asymmetric airfoils. *Journal of Wind Engineering and Industrial Aerodynamics, 179,* 240–249. DOI 10.1016/j.jweia.2018.06.004.

26. Kazachkov, I. (2019). On the modeling of non-classical problems involving liquid jets and films and related heat transfer processes. *Fluid Dynamics & Materials Processing, 15(5),* 491–507. DOI 10.32604/fdmp.2019.06477.

27. Kizito, J., Vander Wal, R., Tryggvason, G. (2004). Effects of splashing droplets on spray cooling processes. *Proceedings of IMECE04. ASME International Mechanical Engineering Congress and Exposition, Heat transfer, 1,* 149–153. Paper No. IMECE2004-59915.

28. Koroteev, A., Bondareva, N., Nagel, A., Filatov, N., Baidenko, I. (2016). Regularities of interaction between drops of UHV coolants and surfaces of traps of frameless heat removal systems in space. *Thermophysics and Aeromechanics, 23(6),* 879–885. DOI 10.1134/S086986431606010X.

29. Bergman, T., Mesler, R. (1981). Bubble nucleation studies. Part I: Formation of bubble nuclei in superheated water by bursting bubbles. *American Institute of Chemical Engineers Journal, 27(5),* 851–853. DOI 10.1002/aic.690270524.

30. Carroll, K., Mesler, R. (1981). Part II: Bubble entrainment by drop-formed vortex rings. *American Institute of Chemical Engineers Journal, 27(5),* 853–856. DOI 10.1002/aic.690270525.

31. Manzello, S., Yang, J. (2003). The influence of liquid pool temperature on the critical impact Weber number for splashing. *Physics of Fluids, 15(1),* 257–260. DOI 10.1063/1.1526696.

32. Lan, M., Wang, X., Zhu, P., Chen, P. (2015). Experimental study on the dynamic process of a water drop with additives impact upon hot liquid fuel surfaces. *Energy Procedia, 66,* 173–176. DOI 10.1016/j.egypro.2015.02.008.

33. Theofanous, T. (2011). Aerobreakup of Newtonian and viscoelastic liquids. *Annual Review of Fluid Mechanics, 43 (1),* 661–690. DOI 10.1146/annurev-fluid-122109-160638.

34. Budko, K., Korshunov, A. (2016). Calorimetric investigation of anomalous heat production in Ni-H systems. *Journal of Condensed Matter Nuclear Science, 22,* 1–6.

35. Williams, A. (1973). Combustion of droplets of liquid fuels: a review. *Combustion and Flame, 21(1),* 1–31. DOI 10.1016/0010-2180(73)90002-3.

36. Fedorchenko, A., Wang, A. (2004). On some common features of drop impact on liquid surfaces. *Physics of Fluids, 16(5),* 1349–1365. DOI 10.1063/1.1652061.

37. Chashechkin, Y. D., Ilinykh, A. Y. (2018). Banded structures in the distribution pattern of a drop over the surface of the host liquid. *Doklady Physics, 63(7),* 282–287. DOI 10.1134/S1028335818070066.

38. Landau, L., Lifshitz, E. (1987). *Fluid mechanics, course of theoretical physics.* vol. 6. Oxford, England: Pergamon Press.

39. Muller, P. (2006). *The equation of oceanic motions.* Cambridge, England: CUP.

40. USF "HPC IPMech RAS" (2018). Unique science facility "Hydrophysical complex for modeling of hydrodynamic processes in the environment and their impact on underwater technical objects, as well as the transport of impurities in the ocean and atmosphere". *http://www.ipmnet.ru/uniqequip/gfk/#equip.*

41. Dalziel, S., Hughes, G., Sutherland, B. (2000). Whole-field density measurements by 'synthetic schlieren'. *Experiments in Fluids, 28(4),* 322–335. DOI 10.1007/s003480050391.

42. Zhang, L., Toole, J., Fezzaa, K., Deegan, R. (2012). Splashing from drop impact into a deep pool: multiplicity of jets and the failure of conventional scaling. *Journal of Fluid Mechanics, 703,* 402–413. DOI 10.1017/jfm.2012.249.

43. Agbaglah, G., Thoraval, M., Thoroddsen, S., Zhang, L., Fezzaa, K. et al. (2015). Drop impact into a deep pool: vortex shedding and jet formation. *Journal of Fluid Mechanics, 764,* R1–12. DOI 10.1017/jfm.2014.723.

44. Chashechkin, Y. D., Prokhorov, V. (2013). Drop-impact hydrodynamics: short waves on a surface of the crown. *Doklady Physics, 58(7),* 296–300. DOI 10.1134/S1028335813070021.

45. Chashechkin, Y. D., Prokhorov, V. (2016). The structure of the primary audio signal in a collision of a free-falling drop with water surface. *Journal of Experimental and Theoretical Physics, 122(4),* 748–758. DOI 10.1134/S1063776116020175.

46. Chashechkin, Y. D., Prokhorov, V. (2017). Acoustics and hydrodynamics of a drop impact on a water surface. *Acoustical Physics, 63(1),* 33–44. DOI 10.1134/S1063771016060038.

47. Chashechkin, Y. D. (2019). Evolution of the fine structure of the matter distribution of a free-falling droplet in mixing liquids. *Izvestiya, Atmospheric and Oceanic Physics, 55(3),* 285–294. DOI 10.1134/S0001433819020026.

48. Feistel, R. (2018). Thermodynamic properties of seawater, ice and humid air: TEOS-10, before and beyond. *Ocean Sciences, 14(3),* 471–502. DOI 10.5194/os-14-471-2018.

49. Gibbs, J. (2010). *Elementary principles in statistical mechanics*. Cambridge, England: CUP.

50. Teschke, O., de Souza, E., (2005). Water molecule clusters measured at water/air interfaces using atomic force microscopy. *Physical Chemistry Chemical Physics, 7(22),* 3856–3865. DOI 10.1039/b511257e.

51. Eisenberg, D., Kauzmann, W. (2005). *The structure and properties of water*. Oxford, England..

52. Chashechkin, Y. (2018). Singularly perturbed components of flows–linear precursors of shock waves. *Mathematical Modelling of Natural Phenomena, 13(2),* 1–29. DOI 10.1051/mmnp/2018007.